General Disclaimer

One or more of the Following Statements may affect this Document

- This document has been reproduced from the best copy furnished by the organizational source. It is being released in the interest of making available as much information as possible.

- This document may contain data, which exceeds the sheet parameters. It was furnished in this condition by the organizational source and is the best copy available.

- This document may contain tone-on-tone or color graphs, charts and/or pictures, which have been reproduced in black and white.

- This document is paginated as submitted by the original source.

- Portions of this document are not fully legible due to the historical nature of some of the material. However, it is the best reproduction available from the original submission.

DEPARTMENT OF GEOPHYSICAL SCIENCES
SCHOOL OF SCIENCES AND HEALTH PROFESSIONS
OLD DOMINION UNIVERSITY
NORFOLK, VIRGINIA

Technical Report GSTR-79-4

A SENSITIVITY ANALYSIS OF VOLCANIC AEROSOL DISPERSION IN THE STRATOSPHERE

By

Carolyn F. Butler

Portions of this work
supported by the
National Aeronautics and Space Administration
Langley Research Center
Under grants
NSG 1343
and
NSG 1477

April 1979

DEPARTMENT OF GEOPHYSICAL SCIENCES
SCHOOL OF SCIENCES AND HEALTH PROFESSIONS
OLD DOMINION UNIVERSITY
NORFOLK, VIRGINIA

Technical Report GSTR-79-4

A SENSITIVITY ANALYSIS OF VOLCANIC AEROSOL DISPERSION IN THE STRATOSPHERE

By

Carolyn F. Butler

Portions of this work
supported by the
National Aeronautics and Space Administration
Langley Research Center
Under grants
NSG 1343
and
NSG 1477

April 1979

ACKNOWLEDGEMENTS

This work is an extension of the authors' Master's Thesis at the College of William and Mary. The principal advisors of this work were Dr. Ellis E. Remsberg of NASA/Langley Research Center and Dr. Jae H. Park of the College of William and Mary. Portions of this research were also discussed with Richard E. Turner and Dr. Patrick Hamill. Portions of this work were supported by the National Aeronautics and Space Administration/Langley Research Center under grants NSG 1343 and NSG 1477.

TABLE OF CONTENTS

LIST OF TABLES

LIST OF FIGURES

LIST OF FIGURES (Cont.)

A SENSITIVITY ANALYSIS OF VOLCANIC AEROSOL DISPERSION IN THE STRATOSPHERE

By

Carolyn F. Butler

ABSTRACT

A computer sensitivity analysis has been performed to determine the uncertainties involved in the calculation of volcanic aerosol dispersion in the stratosphere using a 2-dimensional model. The Fuego volcanic event of 1974 was chosen for this study. Aerosol dispersion processes that were included are: transport, sedimentation, gas phase sulfur chemistry, and aerosol growth. Calculated uncertainties are established from variations in the stratospheric aerosol layer decay times at 37N latitude for each dispersion process. Model profiles are also compared with lidar measurements obtained at the NASA Langley Research Center in Hampton, Virginia (37N).

Results of the computer study are quite sensitive (factor of 2) to the assumed volcanic aerosol source function and the large variations in the parameterized transport between 15 and 20 km at subtropical latitudes. Sedimentation effects are uncertain by up to a factor of 1.5 because of the lack of aerosol size distribution data. Finally the aerosol chemistry and growth, assuming that the stated mechanisms are correct, are essentially complete in several months after the eruption and cannot explain the differences between measured and modeled results.

Don't understand reference system!

1. INTRODUCTION

A characteristic of the earth's stratosphere is a dust layer attributed to volcanic eruptions. This dust layer is made up of liquid or solid aerosols and normally has its peak particle mixing ratio between 18 and 21 kilometers (11). Stratospheric aerosols are predominantly sulfate particles--possibly sulfur dioxide converted through a series of reactions to sulfate and then hydrolyzed to sulfuric acid (5). While the major portion of all stratospheric aerosols is due to volcanic eruptions, other natural and anthropogenic aerosols may contribute to the layer via troposphere-stratosphere exchange processes (24). During periods of low volcanic activity, background concentrations of aerosols are on the order of 0.5 particles per cm^3 or less with sizes ranging from about 0.1 to 1.0 micrometer in radius (12). Particles larger than 1.0 micrometer fall out rapidly by sedimentation and particles smaller than 0.1 micrometer grow by condensation and coagulation processes (30).

While pollutants in the troposphere are quickly dispersed by the winds or removed by rainout (or washout), stratospheric transport processes are weak and stratospheric gases and particulate matter have much longer residence times. Furthermore, this region is close to radiative energy balance and introduction of foreign gases or particles could disrupt the radiative energy budget resulting in climate modification at the earth's surface. The aerosol layer is of particular importance because it resides in the stratosphere. Aerosols affect radiation by both their absorption and scattering properties which are determined, in turn, by various aerosol characteristics such as size, shape and composition. The properties of the stratospheric aerosols and their effect on the radiation balance have been reviewed by Cadle and Grams (1).

In order to adequately assess possible climatic impacts, more must be known about the dispersion and residence times of aerosols following volcanic eruptions. This work considers the dispersion of aerosols from one particular event--the eruption of Mt. Fuego in Guatemala (15N) on 14 and 17 October 1974. Atmospheric transport, particle sedimentation and aerosol physical chemical processes are evaluated for that event by comparing results with observations.

Remote sensing techniques have been used to monitor stratospheric aerosols from ground stations and from aircraft. One such technique, the laser radar (lidar), has been successfully utilized since 1963 to define vertical profiles of aerosol layers. Briefly, the lidar technique consists of a laser transmitter which emits a pulse of light vertically into the atmosphere, where the incident photons are absorbed and scattered by molecules and aerosols. The 180° backscattered light from both the molecular atmosphere and the aerosols is collected by a telescopic receiver located co-linearly with the transmitter. The principle of the lidar and the lidar calibration is described in more detail by Northam, et al. (21) and Remsberg, et al. (33).

A lidar measure of the aerosol mixing ratio is the scattering ratio R_s

$$R_s = 1 + f_a/f_m \qquad (1)$$

where f_a and f_m are the aerosol and molecular backscattering functions, respectively (21). The f-values are products of the species cross-section and number density. The portion of any R_s-value greater than one represents backscattering from aerosols. If the aerosol cross-section is constant with height, the scattering ratio profile is a direct measure of aerosol number density. For an aerosol size distribution which remains constant with time, the stratospheric aerosol

scattering ratio can be used to access the relative change in aerosol number density.

Figure 1 shows two R_s profiles obtained by lidar at Hampton, Virginia. The plot for January 2, 1975, represents an enhanced aerosol layer due to volcanic activity in Guatemala in October 1974 (25). The February 19, 1976, profile resembles a near-background aerosol level and shows the depletion of the January 2 layer over 13 months. As a result of the substantial quantity of lidar data available from Hampton, Virginia (31) and from facilities at other latitudes, an analysis of theoretical models of the latitudinal and vertical dispersion of the stratospheric aerosol layer can be conducted.

The present study involves a sensitivity analysis of the aerosol layer to the various assumptions which are made for the aerosol model in the disperison calculations. Section 2 describes the circulation model and the computational procedure. The aerosol layer processes and the assumptions concerning the aerosol model are explained and justified in Section 3. Gas phase chemistry and aerosol growth effects are also discussed there. Section 4 then describes results of the aerosol sensitivity studies and the validity of those results.

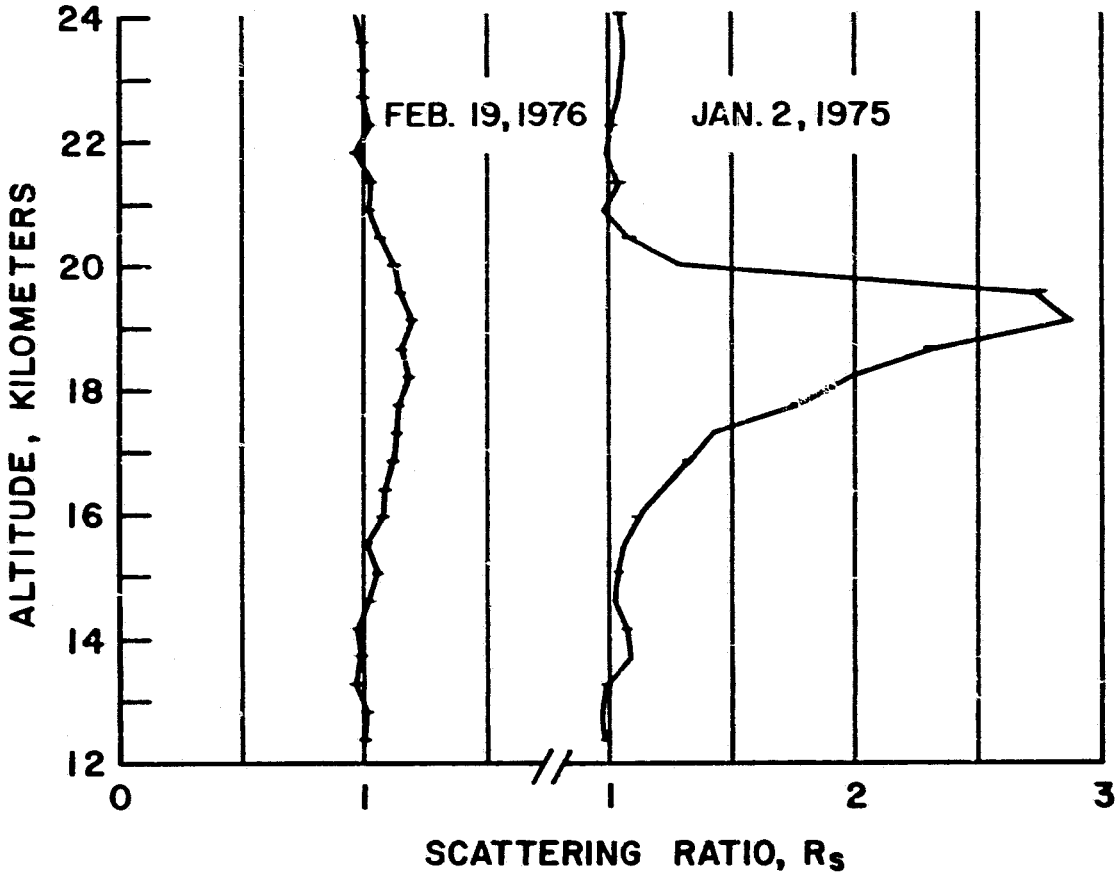

Figure 1. Aerosol scattering ratio profiles from lidar at Hampton, Virginia, following the eruption of Volcan de Fuego in October 1974.

2. MODEL DESCRIPTION

The aerosol distribution is predicted in the form

$$N(t) = N(t_o) + (dN/dt)\ \Delta t \tag{2}$$

where $N(t_o)$ represents the initial aerosol distribution (mass mixing ratio) and Δt is the time step. The rate of change of aerosol mixing ratio dN/dt is defined by

$$\frac{dN}{dt} = \left(\frac{\partial N}{\partial t}\right)_{tr} + \left(\frac{\partial N}{\partial t}\right)_{sed} + \left(\frac{\partial N}{\partial t}\right)_{gr} \tag{3}$$

where $(\partial N/\partial t)_{tr}$ is the transport term, $(\partial N/\partial t)_{sed}$ is the sedimentation term, $(\partial N/\partial t)_{gr}$ is the aerosol growth rate and the gas phase chemistry term.

For simulations presented in this paper, the transport is specifiied by monthly mean winds and eddy diffusion parameters derived from the seasonal circulation in Louis' Model II (18, 2). The model extends from 0 to 50 km in altitude with a verticle grid spacing of 1 km and from 90N to 90S with a horizontal grid spacing of 5 degrees. The continuity equation for the aerosol mass mixing ratio is integrated at specified time steps using a semi-implicit, centered-difference scheme. Louis' model has approximated reasonably the distributions of trace gases and radioactive debris in the stratosphere. In particular, the analysis of a volcanic event represents dispersion from a point source, similar to that for radioactive bomb debris.

The latitudinal boundary conditions are imposed such that there is no flux at the poles. At 50 km the boundary condition allows mass to be advected out of the model, but not diffused out, however, this boundary is well above the aerosol layer and should have little effect on the aerosol dispersion. At the lower boundary, one has the choice of either specifying a constant mass mixing ratio at the boundary or a constant flux through the boundary.

The sedimentation term is simulated by applying fall speeds for various aerosol sizes and a density of 1.5 g cm^{-3}. These aerosol fall speeds have been tabulated by Kasten (14) for several particle sizes and at various altitudes. The assumptions and techniques used to predict the effects of sedimentation will be discussed in detail in section 3.

The gas phase chemistry is considered in terms of its importance to the aerosol mass loading, and subsequent aerosol growth has been incorporated into the model as well. The effects of the chemical and growth term will be discussed in sections 3 and 4.

To initialize and run the model, one must specify an initial gas and aerosol mass distribution, a background gas and aerosol mass distribution, the time step and the lower boundary condition. Initial conditions of aerosol mass distribution $N(t_o)$ for the model are estimated from several data sources. High resolution infrared and visible satellite photographs from SMS (released by the National Oceanic and Atmospheric Administration in Rockville, Maryland) and from the DMSP (U. S. Air Force satellite) are employed to estimate the eruptions of October 14 and 17, 1974 (32). Dust clouds were observed to move to the northeast and to the west. An analysis of rawinsonde profiles obtained at Swan Island (off the east coast of Guatemala) shows winds from the southwest up to about 15 km with a sharp reversal to winds from the east above 16.5 km. Trajectory analysis of dust layers in these two flow regimes explain some of the subsequent observations at higher latitudes (25).

An analysis of the photographs and the local wind profiles indicate that the October 17 event was responsible for the bulk of the 20 km layer; a grid based on that event is used in the model. The model is started on October 19

at 1200Z to allow for some spread of the cloud. Amounts of injected ash and sulfuric acid gas are estimated as a factor of 20 less than the initial distribution for Agung as estimated by Cadle et al. (2). (Cadle, et al. determined the Fuego event to be only a factor of five less than Agung). Data taken by lidar at Hawaii (4) on October 29 are applied to verify the initial vertical profile of the dust layer. The vertical width of the layer at half maximum as computed by the model for October 29 at 20N is compared with the observations (half-width of 0.8 km) at Mauna Loa Observatory in Hawaii for that date. The shape of the model profiles at all altitudes where aerosol had been transported in that 10-day period is adjusted to agree with a zonal average of the Hawaii observations. These adjusted profiles then represent the initial conditions on October 29 for the aerosol source and are shown in figure 2. The sensitivity of the calculations to the specification of the source function is discussed in a subsequent section.

The choice of the initial aerosol size distribution is important for the aerosol sedimentation and growth processes and that distribution is shown in Figure 3. The rationale for this distribution is given in Appendix I. The background aerosol mass mixing ratio is estimated to be 2×10^{-10} and the background sulfuric acid gas concentration is estimated from Figure II-4 in Appendix II.

A time series of dustsonde profiles after the eruption of Fuego shows considerable variation in the aerosol mass mixing ratio in the upper troposphere over Laramie, Wyoming (8). This indicates that mixing of aerosol from the stratosphere to lower altitudes can occur in a non-uniform manner. As a result, the entire tropospheric and stratospheric circulation of Louis' Model II is used and a constant mass mixing ratio of 2×10^{-10} is assumed for the

ALTITUDE (km)	NORTH LATITUDE								
	40°	35°	30°	25°	20°	15°	10°	5°	0°
21		5.4E-10	2.3E-9	8.7E-9	1.6E-8	2.3E-8	2.1E-8	1.2E-8	6.7E-9
20	7.9E-10	2.7E-9	1.2E-8	8.5E-8	8,5E-8	1.23E-7	1.1E.7	6.5E-8	3.6E-8
19		5.4E-10	2.3E-9	8.7E-9	1.6E-8	2.3E-8	2.1E-8	1.2E-8	6.7E-9
18			4.6E-10	1.7E-9	3.2E-9	4.6E-9	4.0E-9	2.4E-9	1.4E-9
17				3.4E10	6.4E-10	9.0E-10	8.0E-10	4.8E-10	2.8E-10

Figure 2. Source input to Louis' Model II on October 29, aerosol mass mixing ratios.

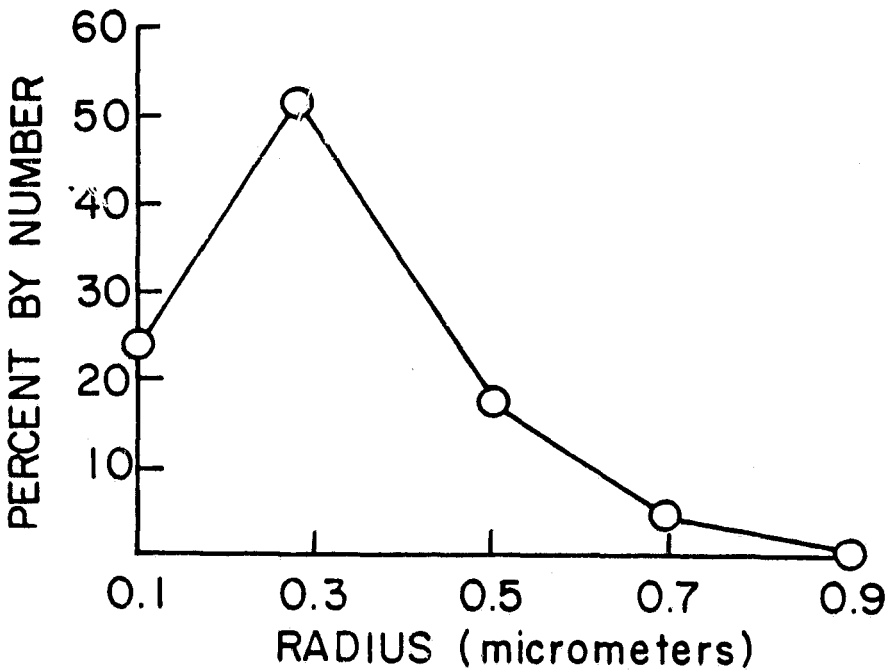

Figure 3. Initial size distribution estimate of Fuego event used in this model.

model at a lower boundary of 2 kilometers.

This time step is chosen such that it is at least an order of magnitude less than the transport relaxation time. This insures stability in the mathematical computations of the continuity equation (eq. 3) (18). The transport relaxation times for the mean winds and eddy diffusion parameters are defined as follows

$$t_v \simeq H_y/v;\ t_w \simeq H_z/w;\ t_{K_{yy}} \simeq H_y^2/K_{yy};$$

$$t_{K_{zz}} \simeq H_z^2/K_{zz};\ t_{K_{yz}} \simeq H_z H_y/K_{yz}$$

where v and w are the latitudinal and veritcal wind components, respectively; y and z refer to the latitudinal and vertical directions, respectively; the K-values are the eddy diffusion coefficients, and; H is the aerosol scale distance over which the mixing ratio changes by 1/e. Initially, the aerosol scale height is small due to the steep graidients of the source, so one hour time steps are used. As the dust disperses, the time step is gradually increased to 12 hours.

3. AEROSOL LAYER PROCESSES

This section deals with each of the processes in equation 3. Even though the gas phase chemistry is not included in the model calculations, assumptions concerning this process are discussed and their effect on the aerosol dispersion is estimated.

A. Transport

The basic equation for time dependent tracer transport is

$$\frac{\partial N}{\partial t} = - V \cdot N + \frac{1}{\rho} \nabla \cdot (\rho K \cdot \nabla N) \qquad (4)$$

where ρ is density of air, V is velocity, ∇ is a gradient operator, K is a second order diffusion coefficient tensor, and N is concentration of the tracer species. The first term on the right of (4) represents advection by the mean winds while the second term represents gradient diffusion. Source and sink terms are expressed separately in equation (3).

The transport term in this modeling attempt is represented by monthly mean winds and eddy diffusion parameters derived from Louis' circulation Model II (18, 2), which adopt the mean winds derived from observations by Newell, et al. (20) below 15 kilometers. Above 15 km the mean winds are computed using the thermodynamic and continuity equations. The eddy diffusion parameters are represented by a tensor coefficient due to physical mixing in the atmosphere and also to the mathematical terms when zonal averaging is performed. The observed distribution of ozone and its observed flux at the ground were used by Louis to adjust the diffusion coefficients with the mean circulation.

The initial assumption in this report is that Louis' Model II has reasonably predicted the dispersion of radioactive bomb debris and therefore should also approximate the dispersion of the volcanic dust layer. Even though this particular

model possesses some deficiencies (largely due to a lack of data sets for parameterizing the circulation), it should be adequate for sensitivity studies of the source function, and of the sedimentation, chemistry and growth terms of equation (3). The sensitivity of the results to the uncertainty in the transport term itself is not addressed explicitly in this study.

It should be noted that the choice of the boundary condition can change the net effect of the mean winds and large-scale eddies. The sensitivity of the model to the boundary condition is tested by varying the boundary from 2 kilometers to 10 kilometers. These results will be discussed in Section 4.

B. Sedimentation

Hunten (9) has discussed the importance of aerosol sedimentation rates for determining the residence times of volcanic aerosol layers. Aerosol fall speeds for various aerosol sizes tabulated by Kasten (14) for particle densities of 1.5 g cm^{-3} are applied to the initial aerosol size distribution derived in Appendix I and plotted in Figure 3. This is a best estimate of the size distribution. An upper limit on the sedimentation rate is obtained with the April 11, 1963 size distribution measurements by Mossop (19) after the eruption of Mt. Agung. Mossop's distributions overestimate the number of larger-sized particles from the Fuego eruption since the Fuego event was not as violent as the Mt. Agung eruption. Mossop's impactor was also biased against the smaller particles. Nevertheless, this data set should at least give an upper limit to the sedimentation rate. A lower limit sensitivity to the sedimentation rate is also tested by applying appropriate fall speeds to a log-normal size distribution representative of a background size distribution of aerosols (23).

The total initial size distribution is divided into five size ranges with mean radii of 0.10, 0.28, 0.50, 0.69 and 0.90 micrometers. Distribution of mass mixing ratios of five different sizes are then calculated as functions of altitude and time.

C. Gas Phase Chemistry

The gas phase chemistry of the SO_2 to aerosol conversion is initially considered with a one-dimensional model to determine its importance in the long-term aerosol dispersion. A simple SO_2 to H_2SO_4 gas phase chemistry is assumed to follow the route

$$SO_2 \rightarrow HSO_3 \rightarrow SO_3 \rightarrow H_2\ SO_4. \tag{5}$$

The specific reactions considered are listed in Table II-I of Appendix II. Junge (13) lists several other reactions that are likely to occur but since the rates of these reactions are unknown and the reaction schemes have not been confirmed, they have not been included. A steady-state model of aerosol gas phase chemistry via (5) is described in Appendix II. The $SO_2 \rightarrow H_2SO_4$ conversion time can be estimated by examining the photochemical relaxation times of reactions 1 through 4 of Table II-I. The photochemical relaxation time is defined as follows

$$t_{ph} = 1/K^* \tag{6}$$

where K^* is the effective reaction coefficient. The effective rate is the product of the number density of the reactant species and the reaction rate. Several assumptions must be made to calculate the effective rates. The reaction rates are not always well known and can vary by orders of magnitude from one reference to another. The concentrations of the reacting gases are sometimes uncertain as well, so one must assume a particular concentration profile. The calculations of the photochemical relaxation times are further complicated by variations of the reaction rates with altitude and time of day. Reaction rates will vary with changing

temperatures and/or the presence of sunlight and certain species concentrations can change by orders of magnitude as a function of altitude. The rate coefficients assumed in this work are listed in Table II-I with references. Park and London (22) have developed a photochemical model including profiles of the species OH, M, O, and HO_2. Their species number densities at 20 km are used to estimate the photochemical relaxation times.

Each phase along the $SO_2 \rightarrow HSO_3 \rightarrow SO_3 \rightarrow H_2SO_4$ route appears to be quite rapid. The rate determining reactions in the SO_2 phase (see Appendix II, Figure II-I) indicate that photochemical relaxation times are on the order of 1 to 10 days. If the uncertainties in the reaction rates and species concentrations are taken into consideration, the relaxation time could be as much as 50 days.

If the amount of SO_2 injected by the Fuego volcano into the stratosphere far exceeded the amount of aerosol injected, then the chemistry term would contribute a major bulk of the aerosol mass to the ambient background layer. However, judging from estimates of Cadle, et al. (2), the eruption cloud contains about equal amounts of SO_2 (or gaseous sulfuric acid) and particulate matter. Since the gas phase chemistry appears to be very rapid, its effects should be small and the chemistry has <u>not</u> been included in the long term dispersion model for calculations of aerosol decay over the order of a year.

D. Gas to Aerosol Conversion and Growth Effects

Aerosol growth by both coagulation and net condensation mechanisms has been evaluated by Turco, et al. (28) and Hamill et al. (30). Coagulation processes cause a change in the size distribution with time, where larger particles grow at the expense of smaller ones. Hamill, et al. (30) show that coagulation is not important for particles with radii greater than 0.2 micrometer. Therefore, coagulation, a process which conserves aerosol mass, is not included in these model calculations.

Condensation, or sulfuric acid gas to aerosol conversion would actually add to the total aerosol mass. The condensation process varies directly with sulfuric acid gas number density and, for a volcanic event, would be a function of altitude. For a layer of aerosol and gas injected at 20 km, the net effect of growth by condensation on the aerosol profile would be to prolong the existence of the aerosol layer.

To simulate the condensation process the growth rates calculated by Hamill (30) are used. These rates are given as a function of altitude and particle radius and they are normalized by the number of molecules of gaseous sulfuric acid present. The parameterization of the growth rates is simplified by choosing those values at 20 km only. Two different sulfuric acid gas profiles are tested with the model--gas mixing ratio values at the source equal to and twice the magnitude of the aerosol source profile (based on estimates by Cadle, et al. (2) of about equal amounts of ash and sulfuric acid injected by Agung). At grid points other than where the volcanic source occurred, a background mass mixing ratio of 6×10^{-15} is used (see Appendix II, Figure II-4). At each time step and grid point and for each of the initial five mean particle radii, particle growth rates are calculated. The change in the mass due to growth is added to the aerosol mass and simultaneously subtracted from the sulfuric acid vapor mass. The sulfuric acid vapor profile is not allowed to fall below the equilibrium value of 6×10^{-15} since it is assumed that the chemical processes (not included in the 2-dimensional model) maintain at least some background amount. The particle size is then updated and a corresponding sedimentation rate is calculated. Results of the growth sensitivity studies are presented in Section 4.

E. Relationship Between Calculated and Observed Mass Densities

The model aerosol distribution is calculated in terms of mass mixing ratio

and this quantity is compared later with lidar backscatter measurements from the aerosol layers. The lidar backscatter results from the product of aerosol number density (which is proportional to aerosol mass) and aerosol backscatter cross section. If the backscatter cross section is constant with time, the trends in the lidar backscatter can be directly compared with the model results.

The aerosol cross section depends on the refractive index, particle shape and size distribution. Measured aerosol samples are predominantly pure liquid spheres (probably sulfuric acid) or ash nuclei coated with liquid, and since the refractive index is determined principally by the outer portion of the aerosol particle, no change in refractive index with time is assumed. Measurements by Hofmann and Rosen (8), however, indicate a changing aerosol size distribution, at least in the early stages of the volcanic dispersion cloud. Remsberg, et al. (33) have analyzed the sensitivity of ruby lidar backscatter returns to various size distribution models and they have determined that this effect is only important for background aerosol size distributions, not volcanic distributions. Therefore, direct comparisons between aerosol mass mixing ratios and lidar backscatter should be valid at least for time periods up to one year after the Fuego eruption.

4. RESULTS OF SENSITIVITY ANALYSES

A. Transport

The sensitivity of $\partial N/\partial t$ to various transport models has not been tested here explicitly even though transport is a dominant term in equation (3). This analysis might be achieved by inputting the Fuego dust source into Louis' other model, Model I (18), in which the mean winds are greater by a factor of 2, or into other available circulation models. Glatt and Widhopf (40), in particular, have applied different radiation and turbulent diffusion models to the calculation of the seasonal meridional circulation patterns according to the formulation of Louis and have then compared their results with those of Louis. That comparison yielded large differences in the tropical and subtropical lower stratosphere, just where the Fuego dust was inserted. In general, their new circulation fields indicated reduced vertical transport at 20 km and a delay in the meridional transport to southern latitudes. It is also possible that the 1974-75 seasonal circulation patterns exhibit differences from those developed from earlier atmospheric data sets by either Louis or Glatt and Widhopf. Due to these differences, circulation patterns and observations of past volcanic eruption clouds are briefly examined instead to determine whether the transport model compares with the general predictions of the Fuego dust route.

According to Lamb (15), the prevailing zonal winds can quickly carry the dust layer around the globe. A typical circuit would take from two to six weeks depending on the latitude of the source. The zonal components of these winds are several orders of magnitude greater than the meridional and vertical components. Therefore, spread of the dust to other latitudes and altitudes should be much lower. The nonsymmetric wave structures of these zonal winds, on the other hand, transport the dust particles in the north-south direction. These processes are represented by

the mean meridional circulation and the large scale eddy diffusion as discussed earlier. The three cell meridional circulation is clearly visible in Louis' model of the winter circulation (Figure 4). Eddy transfers which operate in both directions, appear to dominate the mean circulation in mid-latitudinal spread in winter (see Park and London (22)).

Observations indicate that in late autumn there is a sudden spread of dust into higher latitudinal belts. Dust from the Krakatoa (Indonesia) (May and August, 1883) and Agung (Bali) (February and March 1963) eruptions, both in equatorial latitudes, spreads quickly to about 35N and 35S but was not observed at higher latitudes until late in the following autumn of each hemisphere. In fact, there is evidence that this spread of volcanic dust into other latitude zones is made during the great seasonal circulation changes.

Since the Fuego event occurred in the Northern Hemisphere during the autumn season, one would expect the dust to arrive at the latitude of Hampton, Virginia (37N) in just a few weeks. Observations of past volcanic events shows this to be the case. The eruption of Mt. Agung (8S) occurred during the autumn season of the Southern Hemisphere. The Agung dust was first detected over Melbourne (38S) some 30° to the south in five to seven weeks. Maximum concentrations were observed after about 4 to 6 months at Melbourne but were not observed until one year later after the eruption at latitudes 40-45S where reverse circulation develops. The Fuego dust had only to travel 22 degrees to reach Hampton and, in fact, initial sightings were made in Hampton in 4-6 weeks and maximum concentrations were observed some three months after the eruptions. If we allow for the greater transport distance from Agung to Melbourne compared to Fuego to Hampton and for the lower latitude of the source (8S vs 15N), then the initial appearance of the dust and the time of maximum concentrations compare very well. Remsberg and

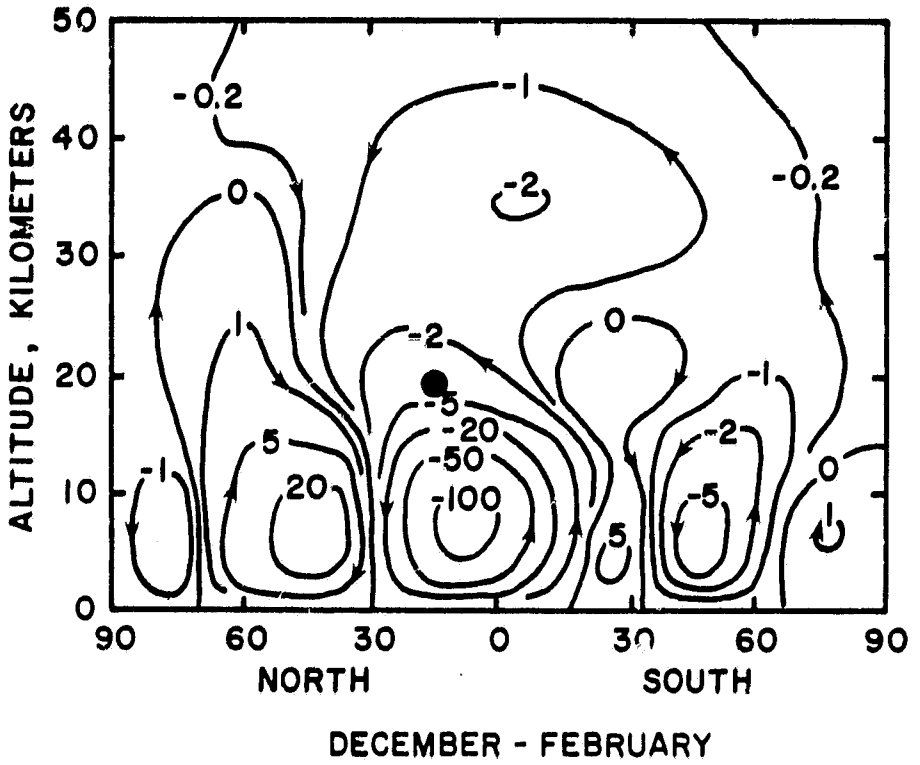

Figure 4. Integrated mass flux (10^{12} g sec^{-1}) from the winter mean circulation of Louis' Model I. The dot represents the altitude and latitude of the initial Fuego volcanic cloud.

Northam (25) have used lower stratosphere circulation maps for October 1974 to explain in more detail the latitudinal spread of the Fuego dust layer.

Figure 5 displays the integrated aerosol mass density from lidar observations at Hampton, Virginia (37N) between 16 and 21 km as a function of time after the eruption. Considerable variability is present in the early returns. The variability in the lidar returns through mid-December represents longitudinal inhomogeneities of the volcanic dust, a feature that cannot be simulated by a zonally averaged model. The integrated lidar data are obtained by summations over 1 km altitude (z) increments of

$$(\bar{R}_s(z) - 1)\, N_m(z) \tag{7}$$

where $\bar{R}_s(z)$ is the average scattering ratio and $N_m(z)$ is the molecular number density (see eq. (1)). Thus, the relative aerosol column density applies to a 5-km column of 1-cm^2 cross section. The quantity on the ordinate is then equivalent to $(\sigma_a/\sigma_m)\, N_a(z)$ where σ_a and σ_m are aerosol and molecular cross sections, respectively, and $N_a(z)$ is the aerosol number density which is directly proportional to aerosol mass density, $M_a(z)$. Therefore, the dimensions of the ordinate in Figure 5 are ML^{-2}. No attempt has been made to actually compute absolute mass densities from the lidar data. That is, no adjustment has been made for possible variations of σ_a with time or altitude, but theoretical studies by Remsberg, et al. (33) indicate no appreciable changes in σ_a for the ruby lidar data.

Figure 6 displays the model integrated aerosol mass density between 16 and 21 km for an average of 35N and 40N latitude. Only the effects of the transport term are considered here. Two curves are generated to determine the sensitivity of the model calculations to the lower boundary condition. A constant aerosol mass mixing ratio of 2×10^{-10} was imposed at 10 km and then on a second run at

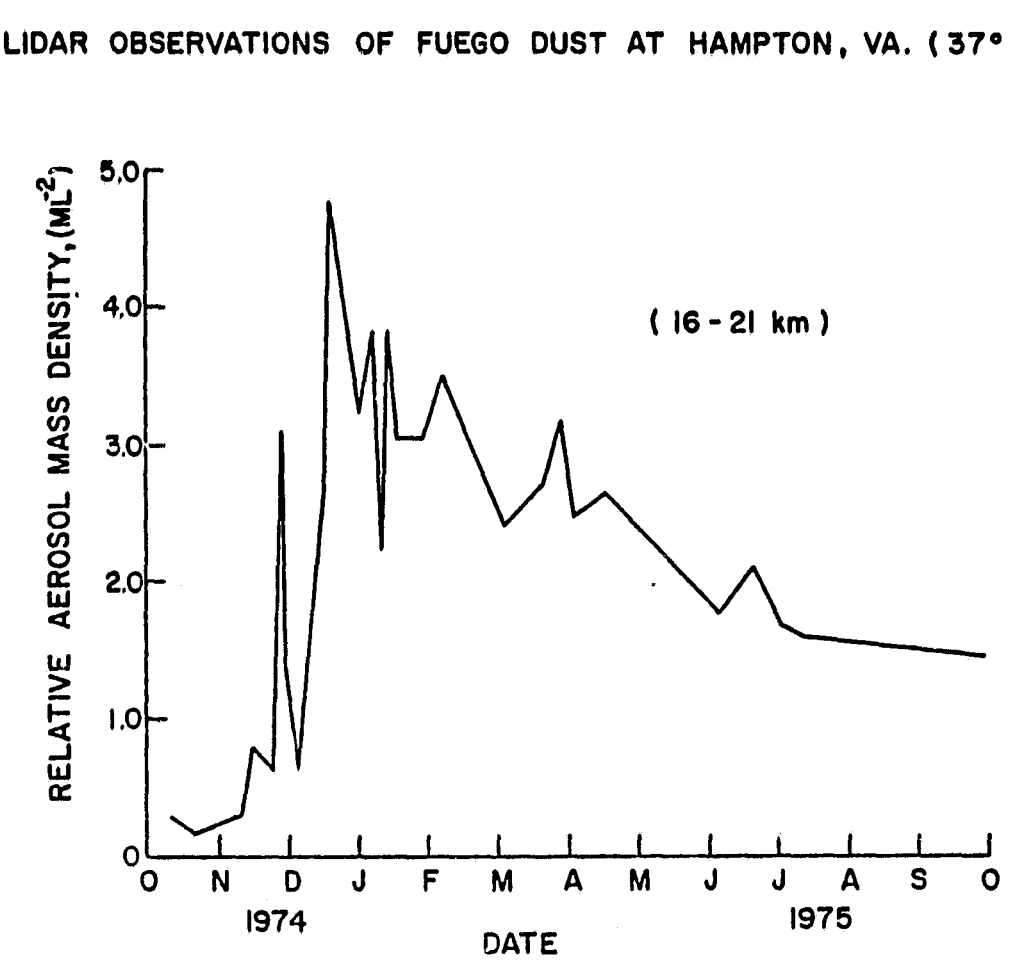

Figure 5. Observed variation of Fuego aerosols at 37N.

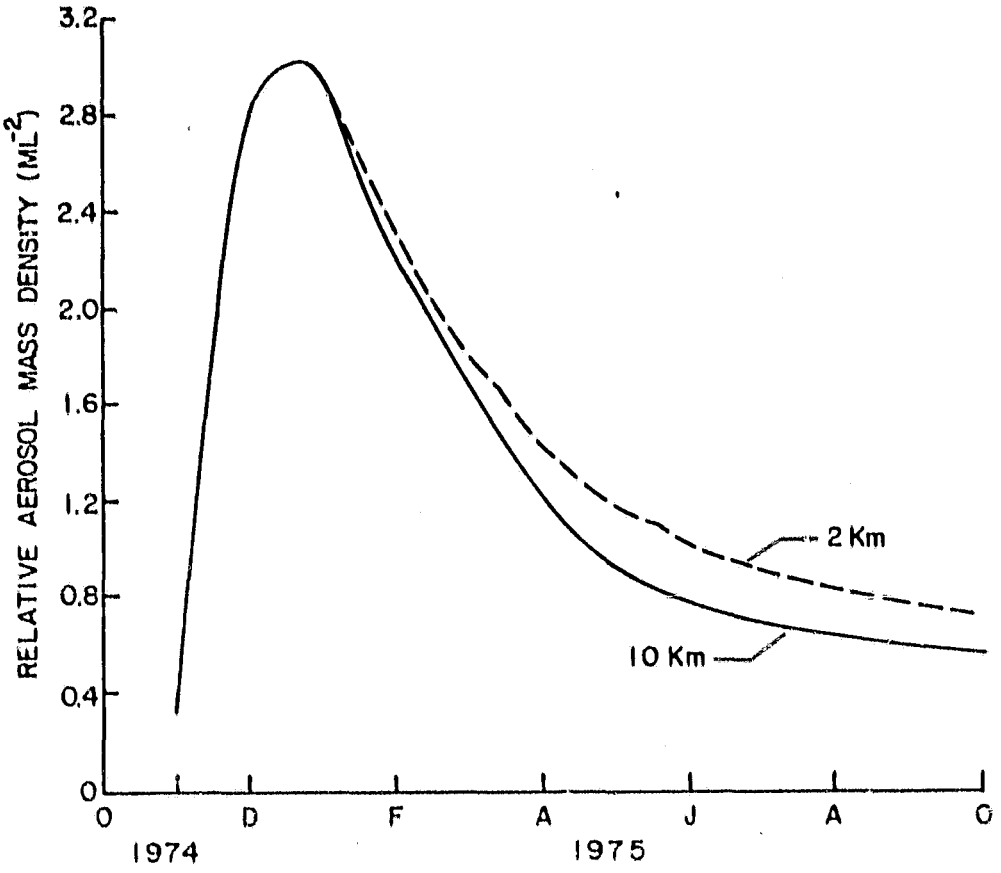

Figure 6. Model sensitivity to lower boundaries of 2 km and 10 km (transport only).

10 km. By setting the boundary by the lower altitude, a decrease occurs in the vertical concentration gradient and the flux across the boundary and into the troposphere, thereby maintaining more mass in the 16 to 21 km column. A 23 percent difference is noted between the two runs one year after the Fuego eruption. The preferred curve is the one for the 2 km boundary. The justification for this choice is based on dustsonde measurements by Hoffman and Rosen (8) indicating a variable rather than a fixed mixing ratio at 10 km altitude from three months after the eruption. This boundary condition also requires a coupled stratosphere-troposphere model such as that which has been applied in this work.

The time of the occurrence of the measured maximum aerosol load at 35N is simulated very well by the model. If the magnitude of the lidar data in Figure 5 and the upper model curve in Figure 6 are normalized to their peak values, the respective time rates of change of the aerosol column are 8 months and 4.5 months.

Figure 7a displays aerosol profiles for 35 to 40N for February and May 1975; the lidar data are plotted in terms of aerosol scattering ratios (a pseudo-aerosol mixing ratio) while the dustonde profiles from the University of Wyoming (8) are in terms of aerosol number density mixing ratios for particles greater than 0.15 micrometer in radius. Although there are some amplitude variations between the lidar and dustsonde data, the mean altitudes of the layer peaks and the widths at half-maximum are comparable. The corresponding model profiles due to only the transport term are presented in Figure 7b and the model profile width at half-maximum is overestimated, which means that either the transport is too rapid or that the source function has been specified improperly. This overestimation is also evident in comparison between model profiles and lidar data at other latitudes.

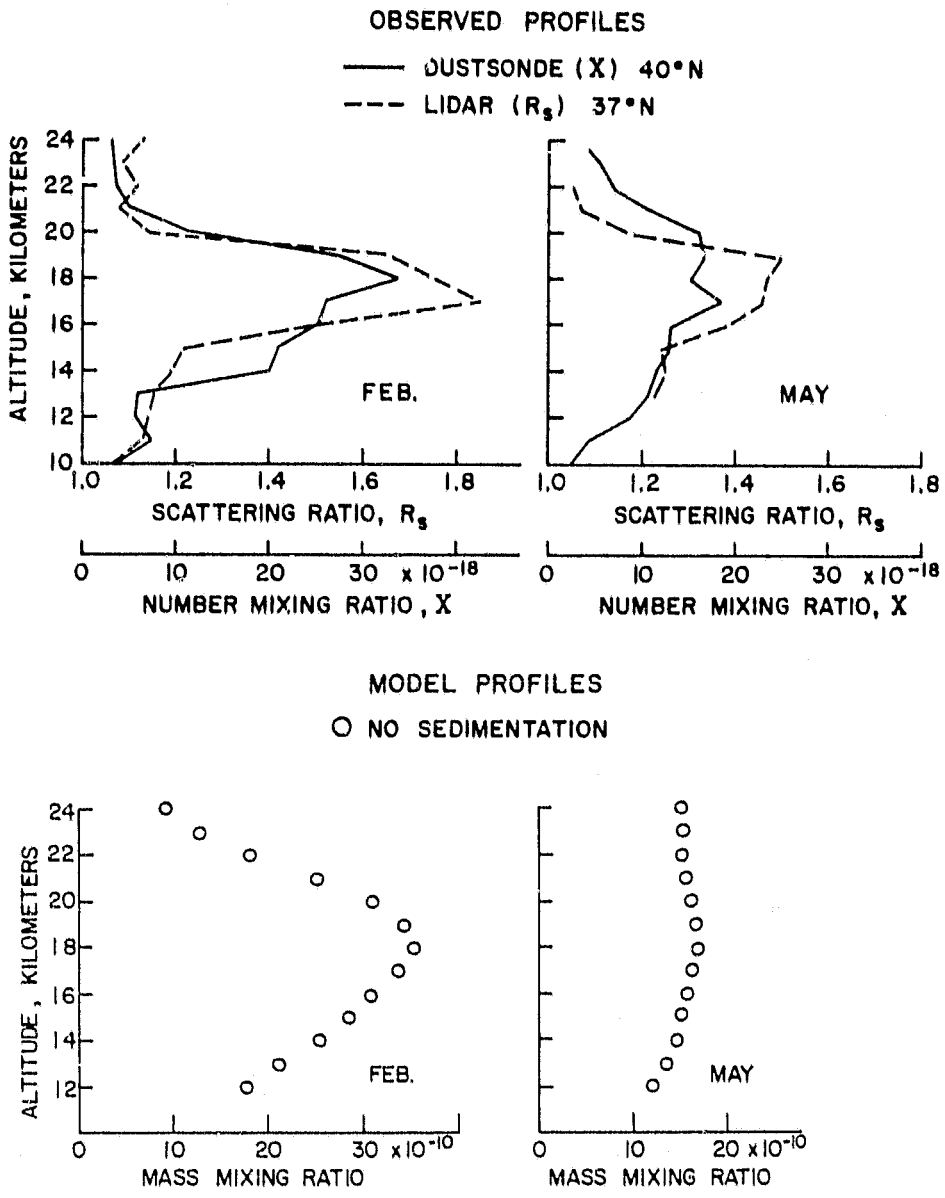

Figure 7a and 7b. Vertical profiles of aerosols from observations and model results for February and May. Units of concentration: Lidar (scattering ratios); dustsonde (number mixing ratios); model (mass mixing ratios). Model lower boundary at 2 km.

If the vertical spread of the model aerosol layer is too rapid then aerosol material will be transported both above and below the 16 to 21 km column. The lidar data do not show significant aerosol above 21 km. The effect of enhanced vertical transport of aerosols by the model is presented in Figure 8 by plotting curves for 16 to 21 km and for 16 to 25 km. One year after Fuego, about 25 percent of the aerosol between 16 and 25 km is above 21 km and the 1/e decay rate is slightly different for the two curves. However, inclusion of the sedimentation term effectively eliminates the spread of material above 21 km and therefore the 16 to 21 km column density curve is selected for all further sensitivity studies in this work.

In conclusion, the transport term appears to represent the meridional transport between 15N and 37N quite well, while overestimating the vertical transport. The uncertainty in the vertical transport which may be due partly to the specification of the source function in the model, has a significant effect on the aerosol dispersion calculation. By inserting the same aerosol source into another 2-dimensional model with the same grid and time step, one could conduct a further check on the uncertainty due to the parameterized circulation as well. That effort is outside the scope of this study.

B. Source Function

The proper specification of a point source event in a zonally averaged model that incorporates gradient diffusion is extremely important but difficult. Louis (18) alluded to this problem when he was formulating his 2-dimensional model and he was forced to consider observations of ozone in order to improve the parameterization of his model. Cadle et al. (2) then applied the model to another point event in the lower stratosphere, the Agung eruption. They adjusted their source function so that the model results agreed with subsequent observations of the

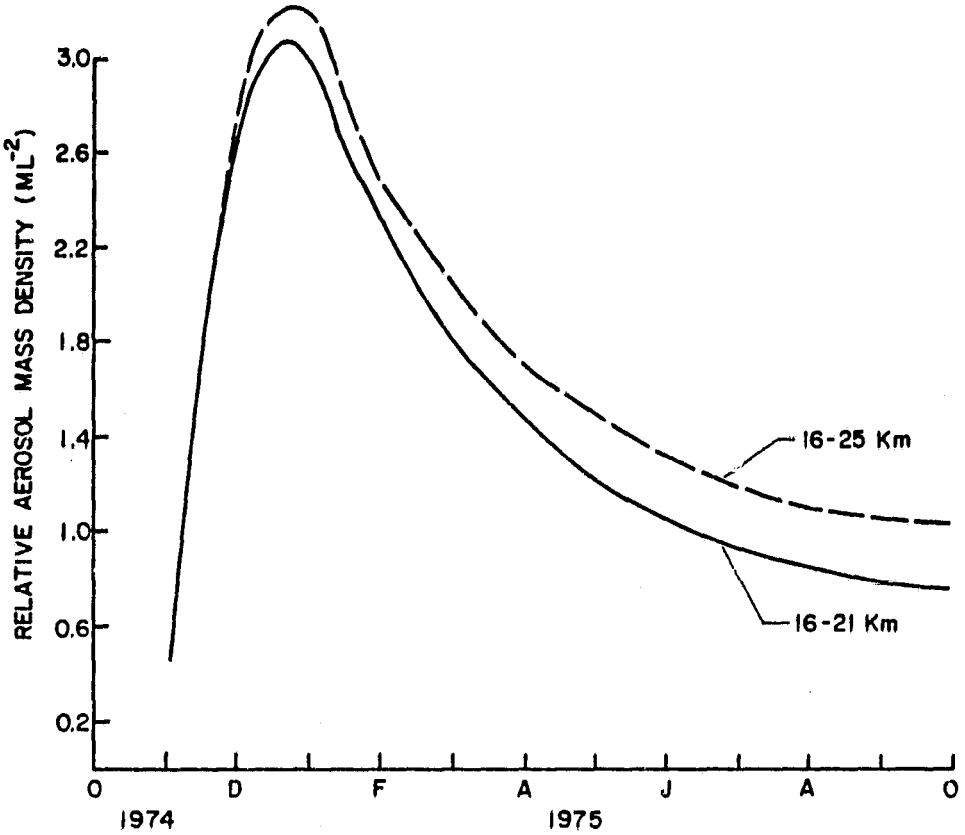

Figure 8. Comparison of model results for the 16-25 km and 16-21 km column loads (transport only).

dust layer at 30N and 40N, latitudes which are far to the north of the source (8S). Their approach required that they assume the circulation to be correct, because the circulation and source function effects could not be decoupled. Thus it is no surprise that their modeled aerosol decay curves agreed with the mid-latitude lidar measurements. Then they further assumed for the Fuego event that the source function was the same as that for Agung, except that the source latitude was moved from 8S to 15N.

To test the sensitivity of the model results to the source function in the present study, the circulation has been assumed correct and several source functions have been tried. The source grid in Figure 2 is thought to have the correct shape but the observations against which it was checked are taken from only one location, Hawaii. Therefore, the zonal averaging process can impart errors to the profile shape, and more important, to the magnitude of the peak mixing ratio.

The shape of the initial vertical profile has been varied, while retaining the same peak mixing ratio, but there are no appreciable differences in the resulting decay curves. No runs were made to test the effects of significantly different source function magnitudes. Although the vertical profile is not resolved very well by the 1 km model grid (39), the dispersion appears to be numerically stable because of the inclusion of the diffusive transport term in the model.

The sensitivity of the advective and diffusive dispersion rate to the assumed initial latitudinal source gradient (see equation 4) has not been tested here, but from Louis' (18) studies it is one of the important uncertainties. The latitudinal gradient from the model run for 60 days after the start date is compared with that published by Cadle et al. (2) and their concentration gradient is weaker. This fact may partially explain why their model decay times are longer than those in the present study. Because the details of their source are not

known, further comparisons with their results are not warranted. In conclusion, the uncertainty in the source function for a 2-dimensional model can only be minimized by waiting about three months after the eruption before initiating the model at which time the longitudinal inhomogeneities are smoothed out and measurements of the latitudinal and vertical concentration gradients are available.

C. Sedimentation

Figure 9 represents the integrated aerosol density between 16 and 21 km as a function of time after the eruption for the case where the sedimentation term is included. The solid curve represents the case where fall speeds were applied to a log-normal background type aerosol distribution (23) of mean radius 0.0726 micrometers. The implication is that the sedimentation term has no effect on a background-type size distribution. The triangles are results for the April 11, 1963 volcanic aerosol size distribution taken from Mossop (19). This distribution contains many large particles which settle out quickly and as such represents an upper limit on the sedimentation effect. The circles represent results for the "best estimate" Fuego initial aerosol distribution shown previously in Figure 3. This distribution is used in the aerosol growth sensitivity studies in the next subsection.

The principal effect of the sedimentation term is to decrease the amplitude of the total curve to shorten the decay time to 2.5 months, and to shift the peak value to the left by about ten days. By not including this term (compare solid curve with circles), one would overestimate the aerosol mass and calculate incorrect decay times. The triangles approach a lower limit in Figure 9, because of the 2×10^{-10} lower limit in mass mixing ratio.

D. Aerosol Growth

Figure 10 presents relative aerosol mass density curves for two conditions

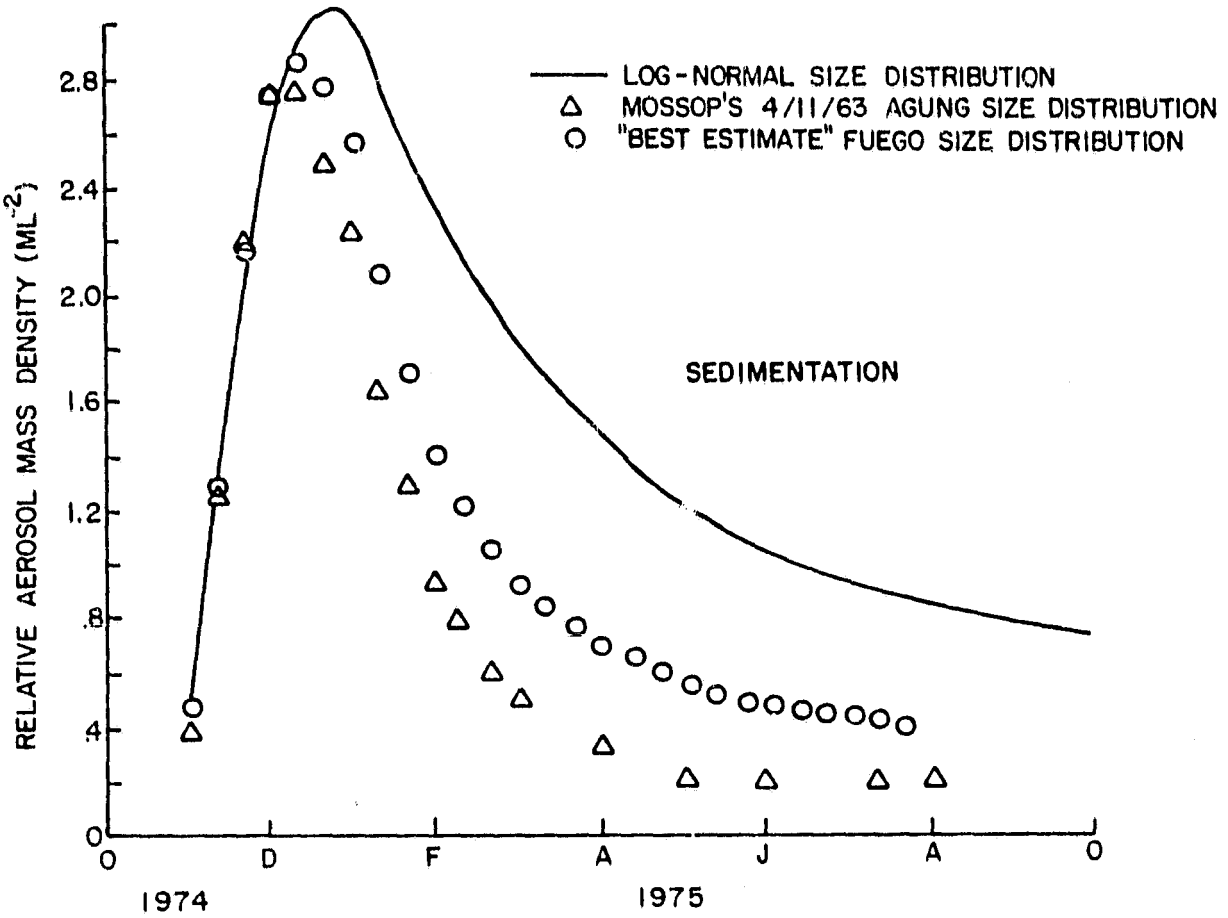

Figure 9. Model results using transport and sedimentation terms.

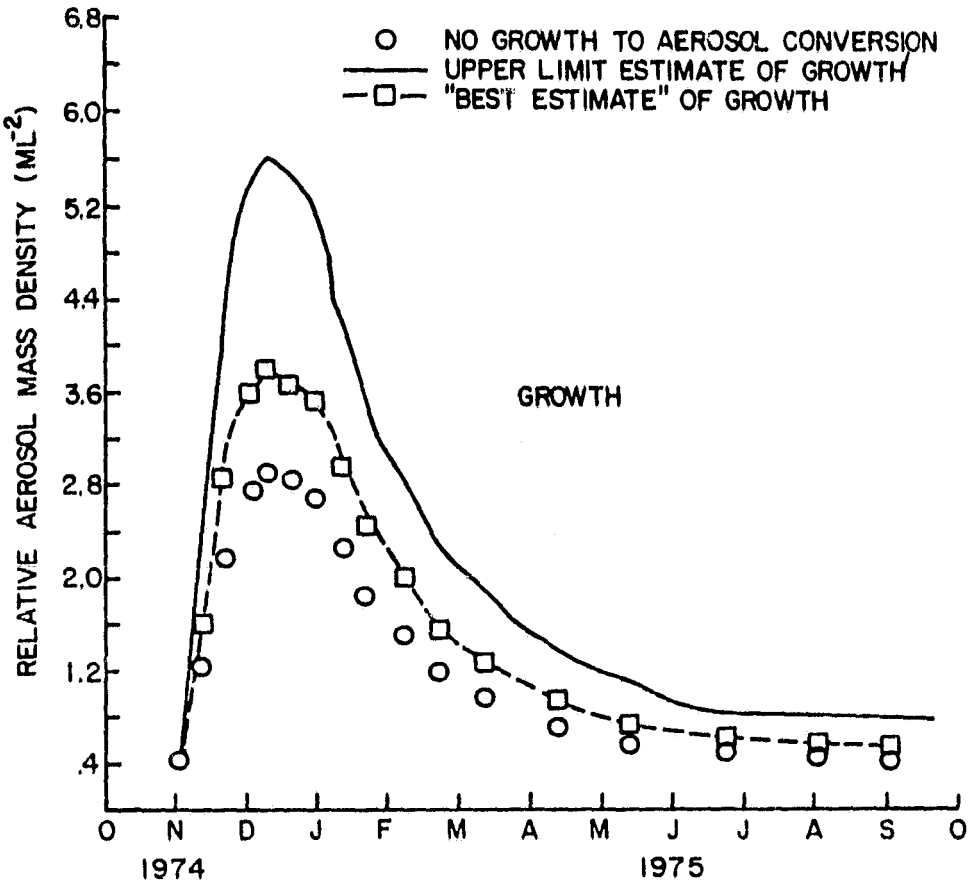

Figure 10. Model results including transport, sedimentation, and condensational growth processes.

1) no gas to aerosol conversion and 2) condensational growth assuming an initial sulfuric acid vapor profile that is equal in magnitude to the sulfuric acid in aerosol phase. Upper limit estimates of the ratio of vapor to aerosol phase sulfuric acid were obtained from Cadle et al. (2) and condensational growth rates were taken from Hamill, et al. (30). Although a growth rate at 20 km was assumed, the rates at the other altitudes between 15 to 25 km vary from it by less than 15 percent for particles with radii between 0.1 and 1.0 micrometers. For a fixed altitude the additional uncertainties in the growth rate equation derived from Hamill et al. (30) have not been modeled, but they are believed to be small because Hamill et al. were able to characterize the background stratospheric aerosol layer quite well using the same expressions. The dashed curve in Figure 10 is a "best estimate" of the effects of growth on the volcanic decay curve and is based on initial sulfuric acid gas to aerosol ratio of one-third. The basis of that estimate is discussed later in this section.

Figure 11 presents the changes in the initial aerosol size distribution curve (Figure 3) at 20 km for three latitudes--35N, 15N, and 25S. Transport, sedimentation, and growth are combined to give these curves. At 15N one finds that the effects of aerosol growth are essentially completed after one month. At 35N the effects of sedimentation compensate those from aerosol growth during the early months and a loss of larger particles by sedimentation is apparent one year later. At 25S only the sedimentation process effects the size distribution, because the volcanic gaseous sulfuric acid is essentially depleted before reaching this latitude. The log-normal background distribution is plotted on that same figure for comparison.

Table 1 lists the number and mass percentages for each size range for both the log-normal and the initial volcanic distribution. The bulk of the aerosol

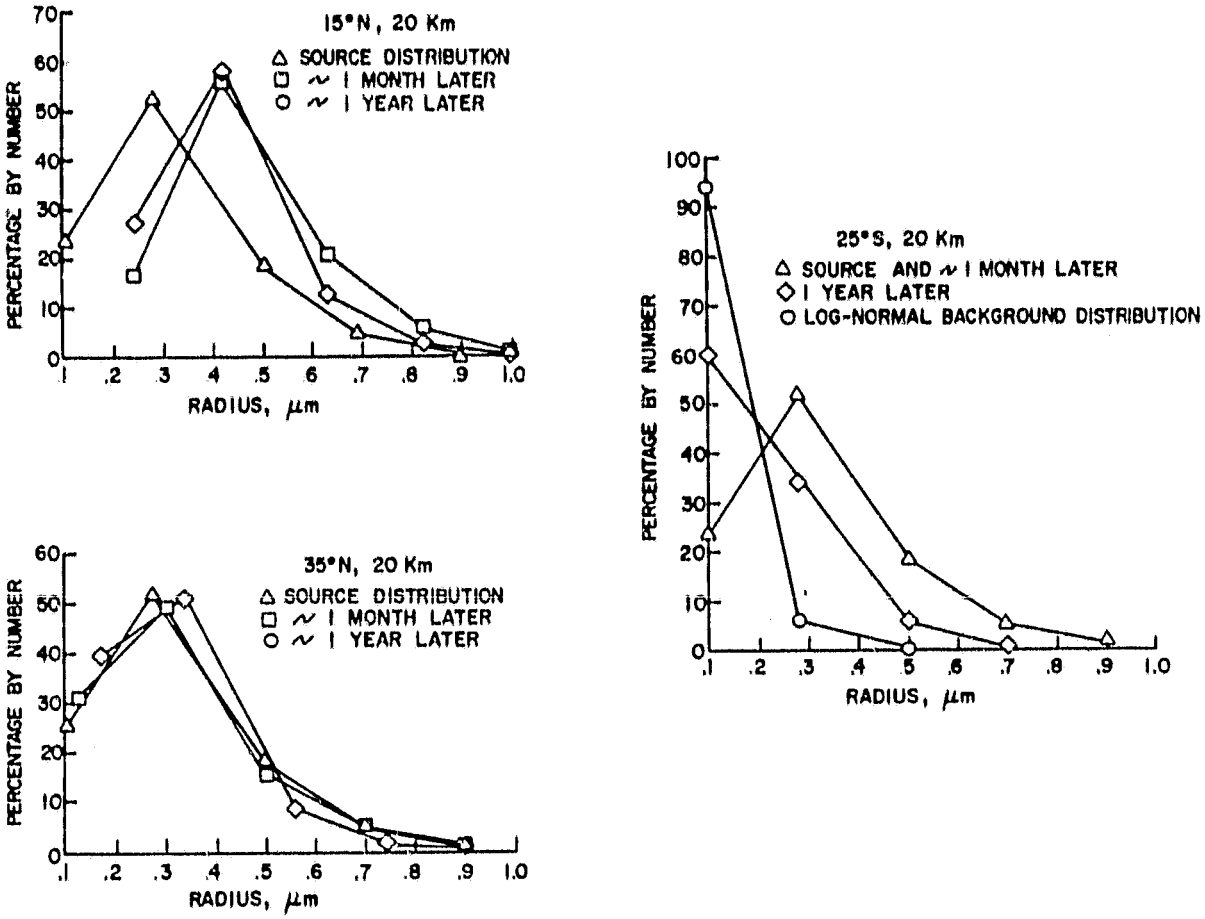

Figure 11. Changes in the initial size distribution curve at 20 km for three model latitudes (35N, 15N, and 25S).

mass occurs at the larger sizes for a volcanic situation. Therefore, any error due to the collection efficiency of the aerosol instruments at 0.1 micrometer is minimized when calculating total aerosol mass density. As a check to the computed effects of condensational growth on the aerosol size distribution curve, Hamill et al. (30) estimate a shift of the curve to larger particles by 0.1 micrometer in about 6 months. Figure 11 (where both condensation and sedimentation are acting) shows that at the latitude of the source, a shift to the right of 0.14 micrometer occurs in one month with little change thereafter. At 35N a shift of 0.07 micrometer is apparent after one year.

Table 1

Stratospheric Aerosol Size and Mass Distribution

Initial Volcanic Distribution			Log-Normal Background Distribution		
Radius	Percent by Number	Percent by Mass	Radius	Percent by Number	Percent by Mass
0.10	24	0.4	0.10	94	30.2
0.28	52	19.7	0.28	5.4	38.1
0.50	18	38.9	0.50	0.5	20.1
0.69	5	28.4	0.69	0.09	9.6
0.90	1	12.6	0.90	0.009	2.1

A comparison has been made in Figure 11c between the model results for Fuego and the observations by Mossop for Agung, both curves for one year after the respective eruptions. Note that the size distribution slope between 0.1 and 0.28 micrometers is greater for the Agung data. This difference exists even though one might expect the opposite because it is probable that there were proportionately more large particles associated with the more intense Agung event. Also by considering the reduced collection efficiency at 0.1 micrometer for Mossop's impactor,

the slope of the observed curve would be even steeper than shown in Figure 11c. To explain this discrepancy, more 0.1 micrometer radius particles must be generated in the model. The calculations presented here do not allow formation of new particles by nucleation and their subsequent growth by coagulation and condensation to the 0.1 micrometer size range. Nucleation, then, represents a possible important process that could be included in the present model if the rate of replenishment of 0.1 micrometer particles could be estimated. Inclusion of this process, however, should have little effect on the resultant aerosol decay curve unless the formation of sulfuric acid vapor is much slower than estimated in Appendix II. A test has been performed where new particles (0.1 micrometers in radius) are allowed to form at a rate equal to the loss due to growth of the particles in the 0.1 micrometer range on the assumption that these smaller particles have a self-preserving property. These "nucleated" particles are then dispersed by the model transport processes but they are not allowed to grow by condensation. As expected, there is no effect on the aerosol decay curve. The size distributions in Figure 11 change considerably, however, with the largest number of particles now in the 0.1 micrometer range at all latitudes.

Model profiles for February and May 1975 at 37N are presented in Figure 12 for the sedimentation and for the sedimentation plus growth cases. These model profiles should be compared with the measured and modeled profiles in Figure 7. Note that the altitude of the maximum aerosol mass mixing ratio is below the 16-21 km range for both cases. A large percentage of the total stratospheric aerosol mass has fallen below the 16 km level and, as a result, the model layer decay time is about 2.5 months. The measured profiles in Figure 7a do not exhibit this rapid depletion of aerosol. The principal reason for this discrepancy is beleived to be the transport in the lower stratosphere in the model.

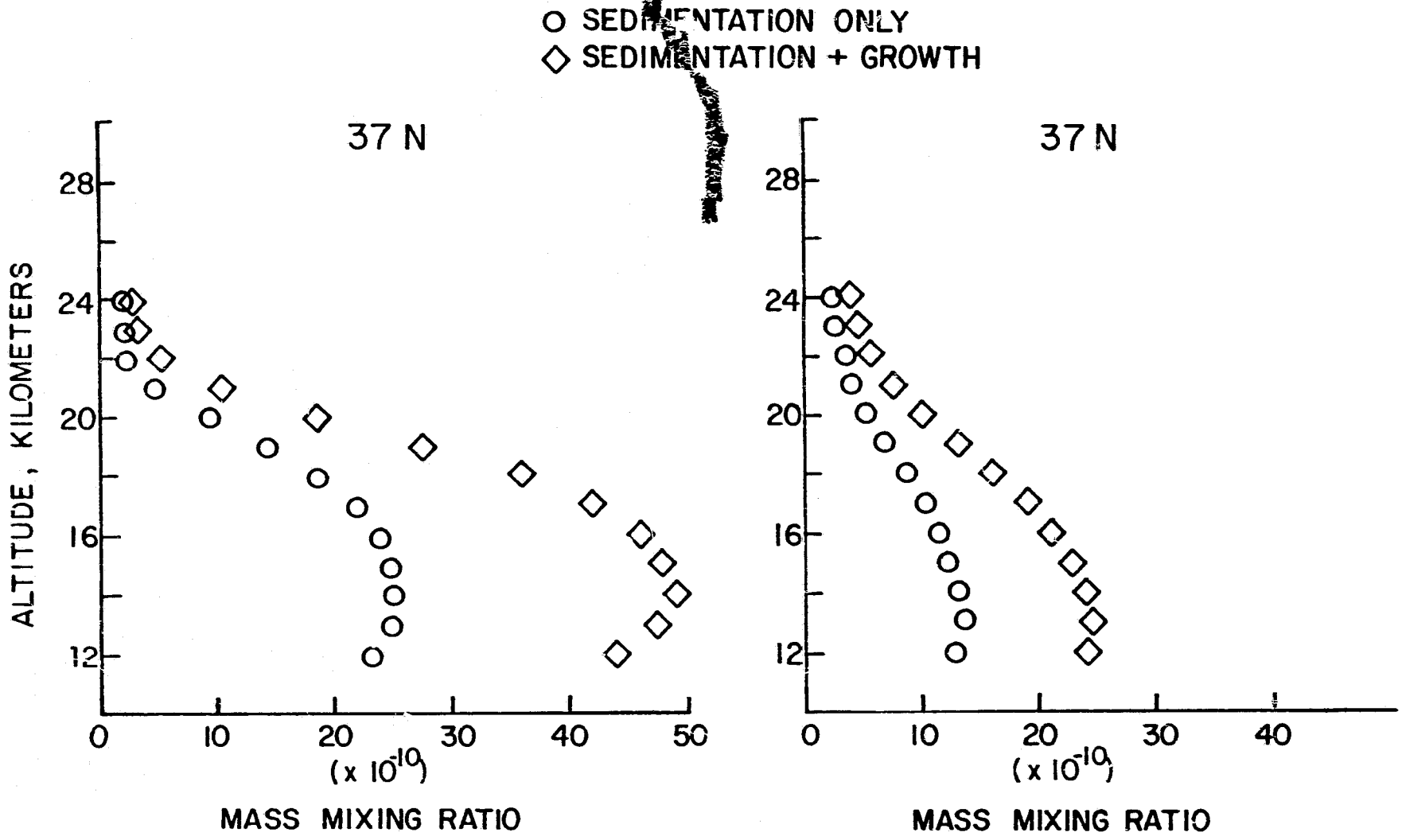

Figure 12. Effects of growth and sedimentation on vertical model profiles.

The rapid growth process, which was complete after several months, agrees with the qualitative conclusions from studies by Hirono et al. (41) and Hoffman and Rosen (8), and from the sulfur isotope data of Castleman (42) for another eruption, Agung. The model sensitivity studies, however, do not support the contention by Hirono et al. (41) that the discrepancy between measured and modeled Fuego decay rates can be accounted for by including aerosol growth in their model studies. A rapid growth process also is at odds with the Agung sulfate concentration data of Castleman, et al. (43) which show maximum concentrations of sulfate occurring about one year after the eruption of the Agung volcano. Even if one assumed that the initial volcanic cloud contained no sulfate particles, one could only support the sulfate trends reported by Castleman et al. (43) by assuming 1) a large sulfuric acid vapor to aerosol ratio at some time following the eruption and/or 2) that the bulk of the sulfate particulate mass is in a size range unaffected by sedimentation. For the first possibility to be true the sulfur dioxide to sulfuric acid gas phase chemistry would have to be much slower than estimated here. Both the chemical mechanism and the reaction rates in Appendix II could be incorrect. The second possibility would require a size distribution with fewer large particles for the sulfate portion of the aerosol layer and perhaps a reassessment of the adequacy of the present condensational growth mechanism. Measurements of the aerosol size distribution for a volcanic cloud in the stratosphere are sparse at best and are subject to large uncertainties. It is also possible that the sampling of the stratospheric aerosol layer during the year after the Agung eruption was too poor to properly account for the expected layering and horizontal inhomogeneties and thus to establish with certainty the trends in total aerosol mass.

To summarize this section, H_2SO_4 gas to aerosol conversion is shown to occur rapidly. If the $SO_2 \rightarrow H_2SO_4$ gas phase conversion is essentially complete after about 10 days, then starting the growth model on October 29 is reasonable. As a result, the 1:1 gas to aerosol ratio estimated from Cadle et al. (2) for the volcanic cloud may be much smaller by the starting date (October 29) for our model runs. Therefore, the best estimate of the growth effects as shown in Figure 10 should be closer to the "no-growth" curve (circles) than to the solid curve. That best estimate is given by the dashed curve in Figure 10. At any rate, the 1/e decay time after January 1975 is relatively unchanged (2.5 months) from the case of no growth. This means that even though the particles gain mass by condensation, they grow larger and are subject to more rapid settling velocities and are therefore lost more quickly from the 16-21 km column.

5. DISCUSSION AND CONCLUSIONS

Figure 13 describes the variation of the 16-21 km curves for 37N latitude. The lidar data in Figure 5 has been fit with a cubic spline function for easier comparison with the model result. The best estimate model aerosol curve is the dashed curve from Figure 10. The measured decay time τ after January 1975 is 8 months. The addition of each term in equation (1) yields: transport only--4.5 months; transport plus sedimentation--2.5 months; and transport, sedimentation and growth--2.5 months. The comparison in terms of Fuego aerosol layer decay times is not particularly good but it is believed to be within the uncertainties of the 2-dimensional model calculation.

By far the largest uncertainty (at least 100 percent) is due to the initial source function and the transport itself. This should not be surprising because it is difficult to obtain the zonal average of a point source function. Also the transport in the lower stratosphere at subtropical and tropical latitudes is particularly deficient because of the sparse data sets and inadequate theory. The sedimentation effect can alter τ by up to 50 percent, because of the lack of good volcanic aerosol size distribution data and to a lesser extent the aerosol density. The sulfuric acid gas phase chemistry and aerosol growth terms do not seem to affect the results. This would not be true, however, if the gas phase chemsitry were much slower than the present 10 day estimate and if the aerosol growth rates were to differ markedly from those for the background stratospheric aerosol layer.

At the onset of this work, it was thought that a sensitivity analysis of the processes affecting the trends in the stratospheric aerosols was necessary to isolate the important deficiencies. That goal has been largly met. In addition, it was felt that the Fuego event might yield a new set of "passive tracer"

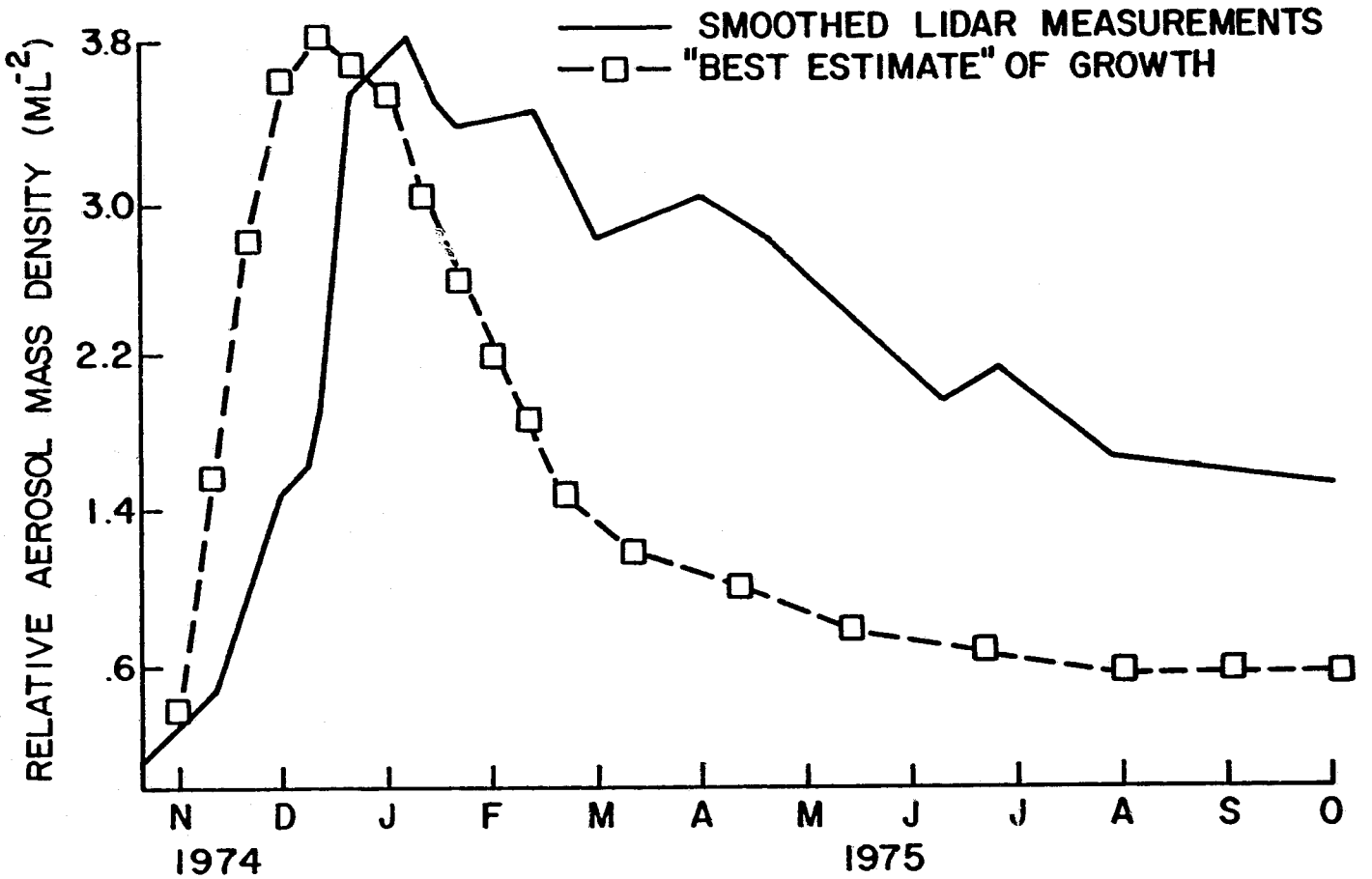

Figure 13. Comparison of smoothed lidar measurements (16-21 km column number densities) over Hampton, VA with best estimate model results.

data for actually validating the circulation in the lower stratosphere. This second goal has not been realized because of the uncertainties associated with the specification of the source function. In order to overcome this problem in the future, the model calculations can be initiated around January 1975 using all available aerosol measurements at that time and when the point source has been more evenly distributed around each latitude zone.

APPENDIX I

Initial Size Distribution Estimate

Stratospheric aerosol size distribution estimates have been critically reviewed by Harris and Rosen (34). Their data summary is applied to primarily non-volcanic material or to volcanic material that has decayed over time periods greater than one year. Five measurements of volcanic aerosols exist in the literature and they are 1) data for the time variation of the Agung dust from Mossop (19); 2) estimates for the size of 0.15 to 0.25 micrometers from the photolectric particle counter of Hofmann and Rosen (8); 3) the data of Miranda and Dulchinos (35) for a January 1975 flight over New Mexico; 4) measurements of the St. Augustine volcanic plume by Hobbs, et al. (36); and 5) data on the volcanic plume of Mt. Baker by Radke, et al. (37). Mossop used an impactor measurement technique while all other data were obtained with some type of optical particle counter. Harris and Rosen (34) and Gras and Laby (38) have evaluated these two techniques with the conclusion that the in situ optical counter is more accurate and does not appreciably affect the physical state of the aerosol.

The measurement by Hofmann and Rosen (8) on December 10, 1974 was processed to yield a Junge-type, $dN/dr = Cr^{-(\nu+1)}$, (11) size distribution slope, $\nu + 1$, of 3.1. This value is strictly applicable to the size range of 0.25 micrometers. That same slope was relatively unchanged on a second flight on February 18, 1975. Due to poor aerosol collection efficiency and the possibility that Mossop's (19) impactor may have been saturated with aerosol material from Agung, data from his impactor is not considered reliable below a radius of 0.3 micrometers, so slopes are obtained from his data over only the range of 0.3 to 0.5 micrometer in radius.

His results vary from a slope of 1.0 on May 28, 1963 to 2.0 on August 6, 1963. On April 2, 1964, one year after the eruption of Agung, Mossop's slope parameter is 4.5. Data from St. Augustine have a mean value of 3.0 and a range of 2.6 to 3.4. Data from Mt. Baker yield values closer to 2.0.

Since most of the aerosol mass is concentrated in the larger particles with radii greater than 0.3 micrometers, it is that size range that must be estimated best. The eruption of Agung was at least a factor of ten stronger than Fuego, according to estimates by Cadle, et al. (2), while the eruptions of Augustine and Mt. Baker were even smaller than that of Fuego. Therefore, it is difficult to know what distribution might be most appropriate for Fuego. As a best estimate the August 6, 1963 particle size distribution of Mossop (19) was selected as representative of the initial condition for Fuego because its slope for particles greater than 0.3 micrometers in radius is 2.0 and that value matches the slope for the distribution in the Mt. Baker plume. This initial distribution is plotted in Figure 3. Another distribution with a slope of 3.0 matches the estimate from data of Hofmann and Rosen obtained two months after the eruption of Fuego and it also agrees with the data of Hobbs, et al. (36) for St. Augustine, a less violent eruption. Clearly more measurements of aerosol size distributions in volcanic dust clouds are needed in the stages just following an eruption, in order to parameterize sedimentation and growth processes in model calculations.

APPENDIX II

Gas Phase Chemistry

In this appendix, a steady-state model of gas phase chemistry is described. The assumption made here is that during periods of non-volcanic activity the background aerosol layer is maintained by conversions from gaseous sulfuric acid.

To develop a chemical model for gaseous sulfuric acid, the following steps are necessary.

1) Determine the possible reactions to be included in the chemical model; and,

2) Determine background concentrations of all reacting species.

A simple SO_2 to H_2SO_4 gas phase chemistry is assumed to follow the path

$$SO_2 \rightarrow HSO_3 \rightarrow SO_3 \rightarrow H_2SO_4$$

Background concentrations for these four gases must be calculated since observed profiles are unavailable. Since these reactions are all assumed to be one-way (i.e., H_2SO_4 is the end-product of SO_2 reactions but H_2SO_4 does not convert back to SO_2) each conversion can be studied as a set of source and sink reactions.

Park and London (22) have developed a photochemical model including reaction and photodissociation rates and species profiles. This particular chemical model was written as a subroutine to Louis' circulation model. The two models are combined in this work to do the chemical calculations. Louis' circulation model is transformed into a one-dimensional model by by-passing the latitudinal computations to save computer time on these preliminary gas phase studies. As previously stated, the eddy diffusion parameters represent not only physical mixing in the atmosphere but also mathematical mixing that occurs when zonal averaging is performed. In

transforming the two-dimensional model, the eddy diffusion parameters reflect the additional mixing due to latitudinal averaging. The vertical diffusion coefficients are assumed to vary from 10^3 - 10^5 cm^2 sec^{-1}.

The continuity equation for a trace gas is written as

$$N(t) = N(t_o) + \left[(\partial N/\partial t)_{ch} + (\partial N/\partial t)_{tr} \right] \Delta t$$

and solved for each time increment. The approach is to assume an $N(t_o)$ and run the model until the quantity N(t) shows only seasonal variations. Then the continuity equation reduces to $(\partial N/\partial t)_{ch} = (\partial N/\partial t)_{tr}$ indicating that the chemical and transport terms have reached equilibrium. The step Δt is chosen such that it is no greater than either the transport relaxation time (see Section 2) or the photochemical relaxation time. Since the chemical processes are faster than the transport processes, time steps are chosen such that they are about one tenth of the chemical relaxation time for the rate-limiting reaction.

To obtain background concentrations of SO_2, reactions (1) to (3) in Table II-1 are considered. The chemical term is then written

$$\partial SO_2/\partial t = - k_1 (SO_2) (OH) (M) - k_2 (SO_2) (O) (M) - k_3 (SO_2) (HO_2) \cdot$$

The dominant reaction can be determined by calculating the effective reaction rate k^* according to $k_1^* = k_1 (OH) (M)$. For the following molecular densities (22)

$$OH = 1.5 \times 10^6 \text{ cm}^{-3} \text{ (at 20 km)}$$

and

$$M = 1.8 \times 10^{18} \text{ cm}^{-3} \text{ (at 20 km)}$$

then

$$k_1^* = 2.2 \times 10^{-6} \text{ sec}^{-1} \text{ (at 20 km, T = 230 K)} \cdot$$

Similarly, for values of $O = 2 \times 10^{6}$ cm^{-3} (22) and $HO_2 \times 10^{7}$ cm^{-3} (22), $k_2^* = k_2 (O) (M) = 2.7 \times 10^{-8}$ sec^{-1} and $k_3^* = k^3 (HO_2) = 1.8 \times 10^{-8}$ sec^{-1}. Reaction (1) is the rate determining reaction in this chemical scheme. The three effective reaction rates, k_1^*, k_2^*, and k_3^* are plotted versus altitude in Figure II-1. The net reaction rates can vary considerably with altitude either due to the change in the rate coefficients with temperature and/or to the change in the density of the reactant gases with altitude (see Figure II-2). Additional errors can be introduced into the calculations of the net reaction rates due to the uncertainties in the rate coefficients and the diurnal change in density of the reactant gases.

Figure II-3 shows the resulting SO_2 profiles after running the model for 100 days using the one-dimensional transport and photochemistry previously discussed. The photochemical model of Park and London supplied the species profiles for the reacting gases OH, M, and HO_2. The SO_2 profiles converge to the 100 day profile as the photochemical and transport terms approach equilibrium. The model is run for another year to verify that any subsequent variations are seasonal. Jaeschke, et al. (10) have measured a value of SO_2 of 145 ng m^{-3} STP for 13 km altitude. This value corresponds to a mixing ratio of 5×10^{-11} which compares very well with the 4×10^{-11} mixing ratio at 13 km predicted by this model.

The formation of HSO_3 in this model occurs through reaction (1). Possible destruction reactions are the following

$$HSO_3 + OH + M \rightarrow H_2SO_4 + M \qquad (4)$$

$$HSO_3 + OH \rightarrow H_2O + SO_3 + M \qquad (5)$$

Reaction rates have not been determined for the HSO_3 destruction terms; however, they are thought to be very rapid (29). Therefore, the net rate of change for the HSO_3 chemistry is assumed to be zero:

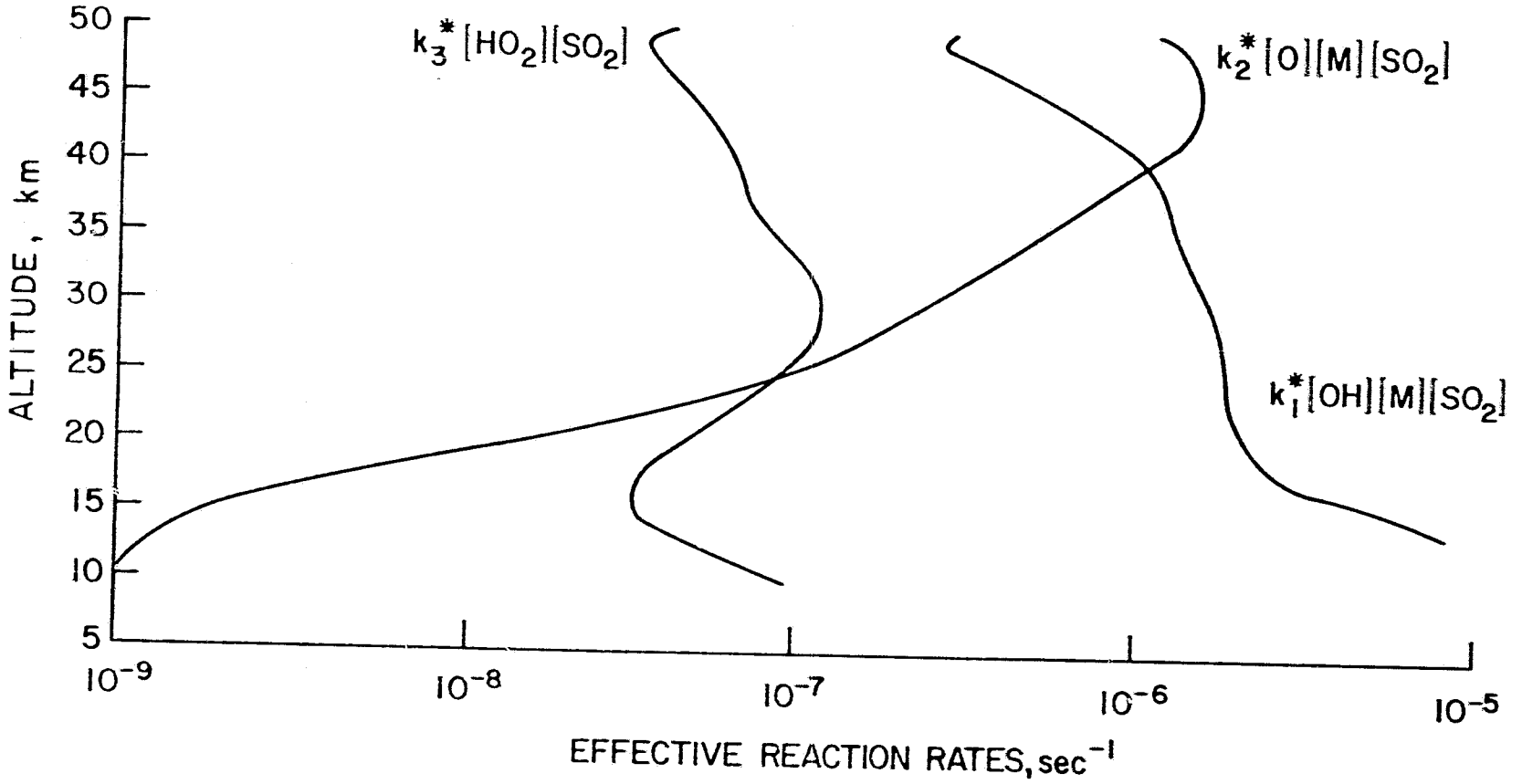

Figure II-1. Effective reaction rates of three SO_2 destruction reactions.

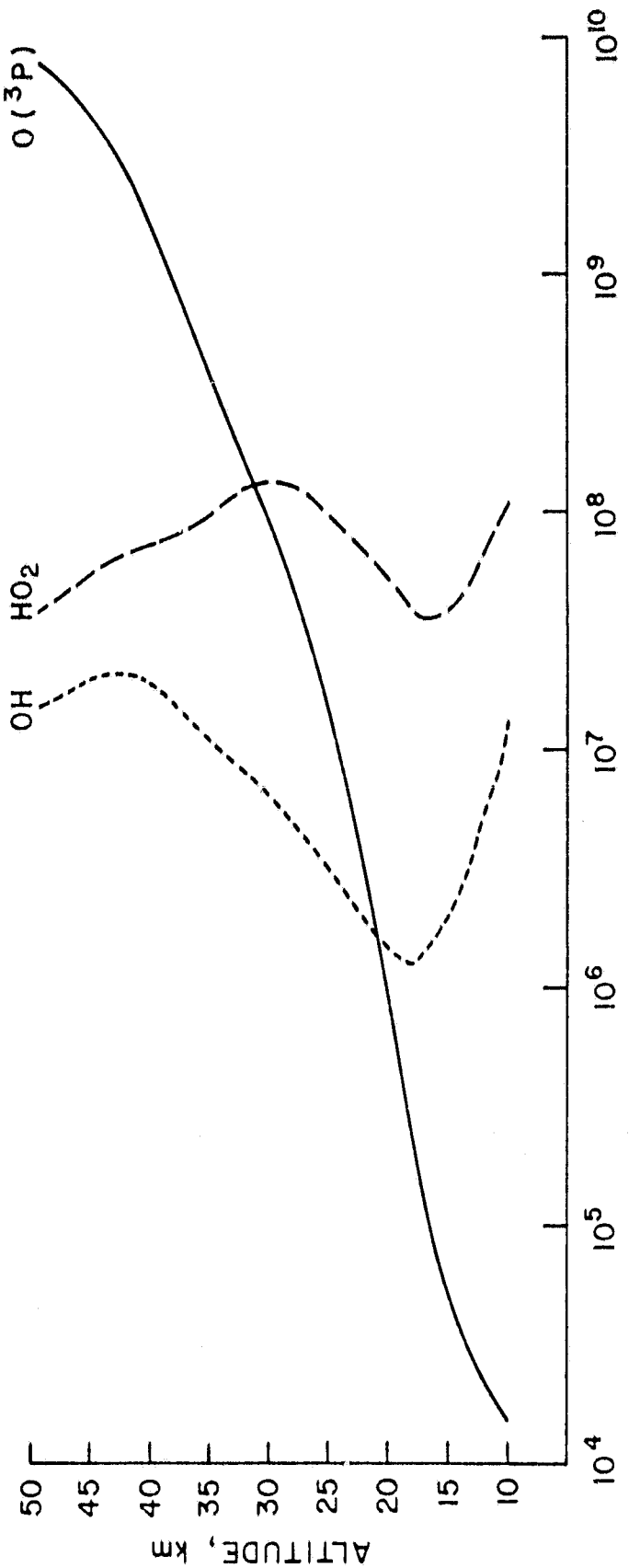

Figure II-2. Molecular densities of the gases $O(^3P)$, OH, and HO_2.

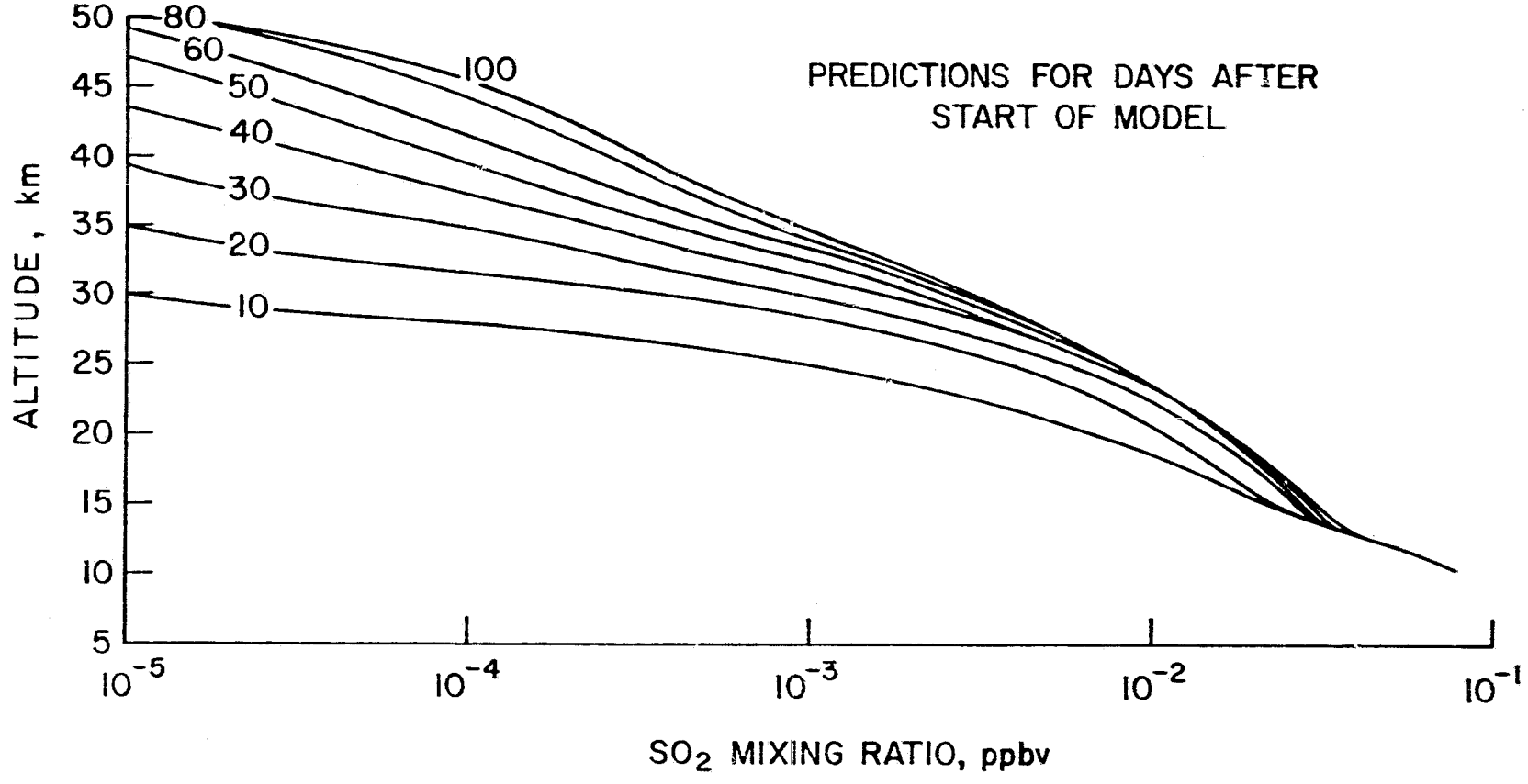

Figure II-3. Model predicitons of SO_2 for various days after start of model.

$$\partial(HSO_3)/\partial t = 0 = k_1\ (SO_2)\ (OH)\ (M) - k_4\ (HSO_3)\ (OH)\ (M)$$

$$-k_5\ (HSO_3)\ (OH)\ (M)$$

which after rearranging terms yields

$$k_4\ (HSO_3)\ (OH)\ (M) = k_1\ (SO_2)\ (OH)\ (M) - k_5\ (HSO_3)\ (OH)\ (M)$$

The SO_3 phase of aerosol gas chemistry can be described by the SO_3 formation reactions (2), (3), and (5) and by the destruction reaction (6) from Table II-1

$$SO_3 + H_2O \rightarrow H_2SO_4 \qquad k_6 = 9 \times 10^{-13}\ cm^3\ mol^{-1}\ sec^{-1}$$

The destruction term has an effective rate of

$$k_6^* = k_6\ (H_2O) = 9 \times 10^{-13} \times 10^{-12} = .91\ sec^{-1}$$

and leads to a destruction of SO_3 that is fast compared to the effective SO_3 formation rates, k_2^* and k_3^*. As in the HSO_3 chemistry,

$$\partial(SO_3)/\partial t = 0 = k_2\ (SO_2)\ (O)\ (M) + k_3\ (SO_2)\ (HO_2)$$

$$+ k_5\ (HSO_3)\ (OH)\ (M) - (SO_3)\ (H_2O)$$

or

$$k_6\ (SO_3)\ (H_2O) = k_2\ (SO_2)\ (O)\ (M) + k_3\ (SO_2)\ (HO_2)$$

$$+ k_5\ (HSO_3)\ (OH)\ (M)$$

The final stage in this particular gas phase chemical scheme is the conversion to sulfuric acid vapor. Reactions (4) and (6) represent the formation terms, and an acid vapor loss rate was determined by imposing boundary conditions from vapor pressure arguments by Hamill, et al. (30).

$$\partial(H_2SO_4) = K_4\ (HSO_3)\ (OH)\ (OH)\ (M) + k_6\ (SO_3)\ (H_2O)$$

The loss rate at the lower boundary, 8 km, of this one-dimensional model, is determined by setting (H_2SO_4) equal to a mixing ratio of 6×10^{-12}, an equilibrium condition between condensed and vapor phase sulfuric acid. This causes a verticle concentration gradient at the lower boundary. The top of the profile, 50 km, was determined by setting (H_2SO_4) equal to 1×10^{-12}. From previous equations the following substitutions can be made

$$\partial(H_2SO_4)/\partial t = k_1\ (SO_2)\ (OH)\ (M) + k_2\ (SO_2)\ (O)\ (M)$$

$$+ k_3\ (SO_2)\ (HO_2)$$

Reactions (1), (2), and (3) determine the H_2SO_4 profile shown in Figure II-4, with the exception of the sharp dropoff below 13 km and above 30 km, both of which are due to the imposed boundary conditions. A total (vapor + aerosol) sulfuric acid profile has been tabulated for comparison from data supplied by Hamill (27). The agreement is reasonable below 30 kilometers. That total curve in Figure II-4 is further broken down into vapor and aerosol profiles to point out that below 30 km all of the sulfuric acid is in condensed form.

As can be seen from Figure II-1, the rate determining reaction for the H_2SO_4 chemistry is reaction (1) (up to 40 km). The effective rate of this reaction is $k_1^* = 2 \times 10^{-6}$ sec^{-1} which corresponds to a relaxation time of 5×10^{-5} sec or about one week. In calculating this relaxation time, one must consider a factor of 2 error for the OH number density. Additional factors of 1.3 for the variation of the number density M and of 2 for the variation in the rate k_1 must be considered for a 10 km layer in the lower stratosphere. This means that the relaxation time for the $SO_2 \rightarrow H_2SO_4$ conversion could be as much as 50 days.

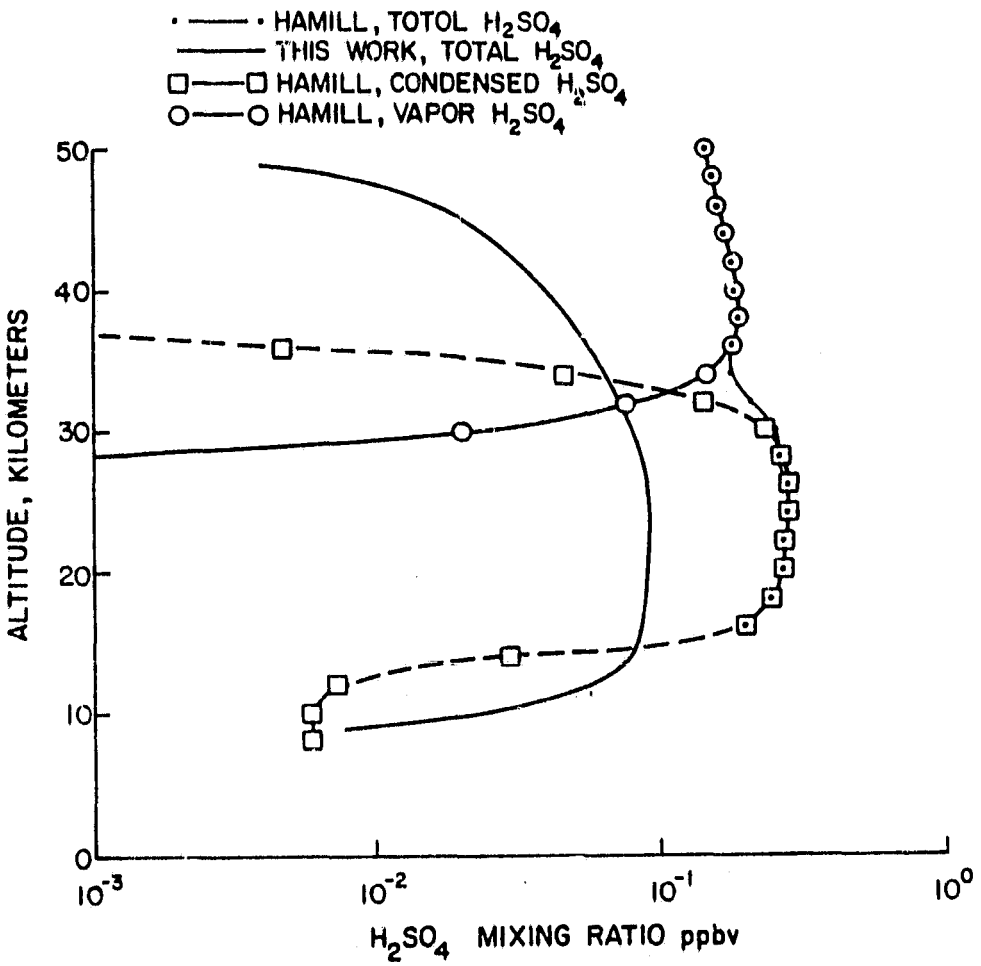

Figure II-4. Model predictions of H_2SO_4.

The condensation of sulfuric acid vapor can be expressed by

$$H_2SO_4 + H_2O \rightarrow H_2SO_4 \cdot H_2O$$

and after n such steps

$$H_2SO_4 \cdot (n-1)\ H_2O + H_2O \rightarrow H_2\ SO_4 \cdot nH_2O$$

Assuming n is 5 or less, the H_2SO_4 predictions, in vapor state, can be compared with aerosol observations (see the vapor and aerosol curves in Figure II-4 from data supplied by Hamill (27).

Some features of this model which play an important role in determining the predicted H_2SO_4 profile are presented in Table II-2. The resulting H_2SO_4 peak concentration (and altitude of the peak) is given in molecules cm^{-3}. The table also shows the assumed values and results used by three other similar steady-state 1-D chemical models. The conversion factors used to determine number densities from the various models are listed in the footnotes.

The parameters presented in Table II-2 affect the resulting sulfuric acid profile in various ways. A larger vertical diffusion coefficient, K_z, will reduce the amount of sulfuric acid produced. The lower boundary condition, which affects the loss rate, and the K_z profile will have a major impact on the resulting altitude for the peak aerosol layer concentration. The dominant reaction $SO_2 + OH + M$ will also affect the altitude of the peak due to the fact that the effective rate is a function of the SO_2, OH, and M profiles. Clearly, SO_2 is the source of sulfuric acid in these models and the amount of sulfuric acid produced will be directly proportional to the magnitude of the SO_2 concentration. The general results of this model then compare well with other published results.

Crutzen (3) suggests that CSO photodissociation in the stratosphere contributes to the stratospheric SO_2 content. However, the CSO chemistry is only invoked to explain the presence of SO_2 in the lower stratosphere in the absence of volcanic activity. It does not affect the ultimate conversion of SO_2 to H_2SO_4.

In Table II-3, the predicted values of H_2SO_4 and $SO_4^=$ at 20 km are presented as well as observed concentrations of $SO_4^=$ and particle mass concentrations. The most extensive observations are those of Lazrus and Gandrud (17) who have made near global measurements of sulfate mass mixing ratios. Their observed $SO_4^=$ can easily be compared to this model's volume mixing ratios by multiplying by the ratio of the molecular weight of air to the molecular weight of $SO_4^=$ (29/96). The 1971 values shown in the table are comparable to their more recent 1974 background values.

All values in Table II-3 have been converted to mass concentrations. The particle concentrations N_p, were converted to mass concentrations M by $M = N_p \pi \rho r^3 4/3$ where valued of r = 0.3 micrometers and $\rho = 1.5$ g cm^{-3} were assumed. The volume mixing ratio in this model was converted to molecular number density and to mass densities according to $M = (N/N_a) \times 98$ where N_a is Avogadro's number and 98 amu is the atomic mass unit weight of sulfuric acid. Aerosol concentrations from Whitten's model (29) have not been tabulated, since the percentage of sulfuric acid that is present in the aerosol phase is not given in his work.

The discrepancy between the 1960 observations of Junge, et al. and of Friend and the later ones reported by Lazrus and Gandrud is not well understood. Lazrus and Gandrud suggest that one possibility may be that the impactor methods used in the earlier samplings are not as efficient in the collection of Aitken-sized particles as the filter type method used in their own studies. Of course, another

possibility is that the differences are real.

In conclusion, results of the steady-state chemistry for sulfuric acid or $SO_4^=$ fall within or close to the range measured by Lazrus and Gandrud for sulfate at 20 km during times of low volcanic activity. An order of magnitude estimate of the relaxation time for the vapor phase chemistry, $SO_2 \rightarrow H_2SO_4$, then is 10 days. From Table II-2, it is important to note the various combinations of parameters which produce the results that are similar to the sulfate observations. Since measurement programs to confirm the proposed gas phase chemistry are lacking, it would be of interest in future studies to determine the limits of the various parameters (within the uncertainties) that would still result in reasonable comparisons with background sulfate observations.

Table II-1

$SO_2 \rightarrow H_2SO_4$ Chemistry and Rates

(1) $SO_2 + OH + M \rightarrow HSO_3 + M$	$k_1 = 1.6 \times 10^{-31}$ cm^{6}mol^{-2}sec^{-1} (T = 300K) $= 8.0 \times 10^{-31}$ cm^{6}mol^{-2}sec^{-1} (T = 230K) (Castleman and Tang, 1977)
(2) $SO_2 + O + M \rightarrow SO_3 + M$	$k_2 = 7.4 \times 10^{-33}$ cm^{6}mol^{-2}sec^{-1} (Mulcahy, et al., 1967)
(3) $SO_2 + HO_2 \rightarrow SO_3 + HO$	$k_3 = 9 \times 10^{-16}$ cm^{3}mol^{-1}sec^{-1} (Payne, et al., 1973)
(4) $HSO_3 + OH + M \rightarrow H_2SO_4 + M$	k_4 = not determined (assumed fast)
(5) $HSO_3 + OH + M \rightarrow H_2O + SO_3 + M$	k_5 = not determined (assumed fast)
(6) $SO_3 + H_2O \rightarrow H_2SO_4$	$k_6 = 9.1 \times 10^{-13}$ cm^{3}mol^{-1}sec^{-1} (Castleman, et al., 1975)

References. The reaction rate (2) listed above is tabulated and referenced in "Chemical Kinetic and Photochemical Data for Modeling Atmospheric Chemistry," NBS TN-866, 1975, and reaction rates for (1), (3), and (6) are tabulated in "Reaction Rate and Photochemical Data for Atmospheric Chemistry--1977," NBS Special Publ. 513, 1978.

Table II-2

Comparative Model Features and Corresponding Results

	K_z ($cm^{-2} sec^{-1}$) (10-50 km)	Lower Boundary (km)	k (SO_2+OH+M) ($cm^6 mol^{-2} sec^{-1}$)	SO_2 (ppb)	Peak Concentration H_2SO_4 or $SO_4^=$ ($mol\ cm^{-3}$)	
Figure II-4	$4 \times 10^4 - 5 \times 10^5$	8	1.6×10^{-31}	.013 (at 20 km) .1 (at 10 km)	5.5×10^7 (at 16 km)	(a)
Harrison and Larson (7)	5×10^3	15	1.0×10^{-31}	1.0 (at 15 km)	1.7×10^9 (at 18 km)	(b)
Harker (6) case 1	$2 \times 10^3 - 3 \times 10^5$	15	1.0×10^{-31}	.2 (at 15 km)	4.7×10^8 (at 18 km)	(b)
case 2	$4 \times 10^3 - 5 \times 10^4$	10	1.0×10^{-13}	.2 (at 10 km)	8.4×10^8 (at 12 km)	(b)
case 3	$1 \times 10^4 - 1 \times 10^5$	10	1.0×10^{-31}	.2 (at 10 km)	6.9×10^8 (at 12 km)	(b)

(a) Calculated as H_2SO_4 vapor mixing ratio. To convert from mixing ratio to molecular concentration, multiply by air density at 16 km ($3.5 \times 10^{18}\ cm^{-3}$).

(b) Calculated as $SO_4^=$ mass concentration. To convert to molecular concentration, multiply by Avogadro constant and divide by molecular weight of sulfate (96 amu).

Table II-3

Comparative Results Between Model Predictions and Observations for Sulfate Mass Concentrations at 20 km

Model	Sulfate Mass Concentration (at 20 km)
	g cm^{-3}
Harrison and Larson (7)	2.6×10^{-13}
Harker (6)	6.0×10^{-14}
This model	7.1×10^{-15}
Measurements	
Junge, et al., (1961) (11) (particle concentration)	1.3×10^{-14}
Junge and Manson (1961) (12) ($SO_4^=$ mass concentrations)	6.8×10^{-15}
Friend (1966) (5) (particle concentrations)	5.2×10^{-15}
Lazrus (1971) (16) ($SO_4^=$ mass concentrations)	$4.2 \times 10^{-14} - 1.1 \times 10^{-13}$

REFERENCES

1. Cadle, R. D. and G. W. Grams. "Stratospheric Aerosol Particles and Their Optical Properties," Rev. Geophys. Space Phys., 13 (1975), 475-501.

2. Cadle, R. D., C. S. Kiang, and J. F. Louis. "The Global-Scale Dispersion of the Eruption Clouds from Major Volcanic Eruptions," J. Geophys. Res., 81 (1976), 3125-3123.

3. Crutzen, P. J. "The Possible Importance of CSO for the Sulfate Layer of the Stratosphere," Geophys. Res. Lett., 3 (1976), 73-76.

4. Fegley, R. W. and H. T. Ellis. "Lidar Observations of a Stratospheric Dust Cloud Layer in the Tropics," Geophys. Res. Lett., 2 (1975), 139-141.

5. Friend, J. P., R. Leifer, and M. Trichon. "On the Formation of Stratospheric Aerosols," J. Atmos. Sci., 30 (1973), 465-479.

6. Harker, A. "The Formation of Sulfate in the Stratopshere Through the Gas Phase Oxidation of Sulfur Dioxide," J. Geophys. Res., 80 (1975), 3399-3401.

7. Harrison, H. and T. Larson. "The Oxidation of SO_2 in the Stratosphere," J. Geophys. Res., 79 (1974), 3095-3097.

8. Hofmann, D. J. and J. M. Rosen. "Balloon Observations of the Time Development of the Stratospheric Aerosol Event of 1974-1975," J. Geophys. Res., 82 (1977), 1435-1440.

9. Hunten, D. "Residence Times of Aerosols and Gases in the Stratosphere," Geophys. Res. Lett. 2 (1975), 26-28.

10. Jaeschke, W., R. Shmitt, and H. W. Georgii. "Preliminary Results of Stratopsheric SO_2 Measurments," Geophys, Res. Lett., 3 (1976), 517-519.

11. Junge, C. E., C. W. Chagnon, and J. E. Manson. "Stratospheric Aerosols," J. Meteorol., 18 (1961), 81-108.

12. Junge, C. E. and J. E. and J. E. Manson. "Stratospheric Aerosol Studies," J. Geophys. Res., 66 (1961), 2163-2182.

13. Junge, C. E. "Sulfur Budget of the Stratospheric Aerosol Layer," Proc. of the Int. Conf. on Structure, Composition and General Circulation of the Upper and Lower Atmospheres and Possible Anthropogenic Perturbations, Univ. of Melbourne, Australia, Jan. 14-25, 1974, 85-100.

14. Kasten, F. "Falling Speed of Aerosol Particles," J. Appl. Meteorol., 7 (1968), 944-947.

15. Lamb, H. "Volcanic Dust in the Atmosphere; With a Chronology and Assessment of its Meteorological Significance," Phil. Trans. Roy. Soc. London, 266A (1970), 425-533.

16. Lazrus, A. L., B. Gandrud, and R. D. Cadle. "Chemical Composition of Air Filtration Samples of the Stratospheric Sulfate Layer," J. Geophys. Res., 76 (1971), 8083-8088.

17. Lazrus, A. L. and B. W. Gandrud. "Stratospheric Sulfate Aerosol." J. Geophys. Res. 79 (1974), 3424-3431.

18. Louis, J. F. "A Two-Dimensional Transport Model of the Atmosphere," Ph.D. Thesis, Univ. of Colorado, 1974.

19. Mossop, S. C. "Volcanic Dust Collected at an Altitude of 20 km," Nature, 203 (1964), 824-827.

20. Newell, R. E., D. G. Vincent, T. G. Dopplick, D. Ferruza, and J. W. Kidson. "The Energy Balance of the Global Atmosphere," The Global Circulation of the Atmosphere, G. A. Corby (Ed.), Roy. Meteorol. Soc., London, 1969.

21. Northam, G. G., J. M. Rosen, S. H. Melfi, T. J. Pepin, M. P. McCormick, D. J. Hofmann, W. H. Fuller, Jr. "A Comparison of Dustsonde and Lidar Measurements of Stratospheric Aerosols," Appl. Opt., 13 (1974), 2416-2421.

22. Park, J. H. and J. London. "Ozone Photochemistry and Radiative Heating of the Middle Atmosphere," J. Atmos. Sci., 1898-1916, 1974.

23. Pinnick, R. G., J. M. Rosen and D. J. Hofmann. "Stratospheric Aerosol Measurement III: Optical Model Calculations," J. Atmos. Sci., 33 (1976), 304-314.

24. Reiter, E. R. "Stratospheric-Tropospheric Exchange Processes," Rev. Geophys. Space Phys., 13 (1975), 459-474.

25. Remsberg, E. E. and G. B. Northam. "A Comparison of Dustonde and Lidar Measurements of Stratospheric Aerosols," Proc. of Fourth Conf. on the Climatic Impact Assessment Program (CIAP), DOT (1976), 509-518.

26. Rosen, J. M., D. J. Hofmann, and P. Singh. "A Steady-State One Dimensional Model of the Stratospheric Aerosol," NASA CP-2004, Dec. 1976.

27. Hamill, P., Institute for Atmospheric Optics and Remote Sensing, Hampton, Virginia, private comm., 1978.

28. Turco, R. P., Hamill, O. B. Toon, and R. C. Whitten. "A Model of the Stratospheric Sulfate Aerosol," NASA CP-2004, Dec. 1976.

29. Whitten, R. C. and R. P. Turco. "Gas Phase Chemistry in the Ames Stratospheric Aerosol Model," NASA CP-2004, Dec. 1976.

30. Hamill, P., O. B. Toon and C. S. Kiang. "Microphysical Processes Affecting Stratospheric Aerosol Particles," J. Atmos. Sci., 34, (1977), 1104-1119.

REFERENCES (Cont.)

31. McCormick, M. P., T. J. Swissler, W. P. Chu and W. H. Fuller, Jr. "Post-Volcanic Stratospheric Aerosol Decay as Measured by Lidar," J. Atmos. Sci., 35, (1978), 1296-1303.

32. Remsberg, E. E., C. F. Jones and J. H. Park. "A Two-Dimensional Model of the Disperison of Aerosols from the Fuego Eruption," NASA CP-2004, Dec. 1976.

33. Remsberg, E. E., G. B. Northam and C. F. Butler. "Lidar Backscattering Measurements of Background Stratospheric Aerosols," NASA Technical Paper 1381, 1979.

34. Harris, F. S. and J. M. Rosen. "Measured and Analytic Distribution of Stratospheric Aerosols: A Review and Commentary," NASA CP-2004, Dec. 1976.

35. Miranda, H. A., Jr. and J. Dulchinos. "Balloon Measurements of Stratospheric Aerosol Size Distribution Following a Volcanic Dust Incursion," AFCRL-TR-75-0518, August 1974.

36. Hobbs, P. V., L. F. Radke and J. L. Stith. "Eruptions of the St. Augustine Volcano: Airborne Measurements and Observations," Science, 195, (1977), 871-873.

37. Radke, L. F., P. V. Hobbs and J. L. Stith. "Airborne Measurements of Gases and Aerosols from Volcanic Vents on Mt. Baker," Geophysical Res. Letters, 3, (1976), 93-96.

38. Gras, J. L. and J. E. Laby. "Southern Hemisphere Stratospheric Aerosol Measurements 1. Simultaneous Impactor and In Situ Single-Particle (Light Scatter) Detection," J. Geophys. Res., 81, (1978), 1869-1874.

39. Mahlman, J. D. and R. W. Sinclair. "Tests of Various Numerical Algorithms Applied to a Simple Trace Constituent Air Transport Problem," in Fate of Pollutants in the Air and Water Environments, Part 1, volume 8, edited by Irwin H. Suffet. John Wiley & Sons, Inc., (1977) 223-252.

40. Glatt, L. and G. F. Widhopf. "Aircraft HO_x and NO_x Emission Effects on Stratospheric Ozone and Temperature," NASA Contractor Report 158945. The Aerospace Corporation, El Segundo, CA. (1978).

41. Hirono, M., M. Fujiwara, T. Itabe and C. Nagasawa. "On the Long Term Variations of Stratospheric Aerosol Content after the Eruption of Fuego Volcano Observed by Lidar," J. Geomag. Geoelectr., 29, (1977) 541-556.

42. Castleman, A. W., Jr., "Nucleation processes and Aerosol Chemistry," Space Sci. Rev., 15, (1974) 547-589.

43. Castleman, A. W., Jr., H. R. Munkelwicz and B. Manowitz. "Isotope and Concentration Measurements of Stratospheric Sulfate," Proc. of the Int. Conf. on Structure, Composition and General Circulation of the upper and Lower Atmospheres and Possible Anthropogenic Perturbations, Volume I, Melbourne, Australia, (1974), 119-127.

44. Cadle, R. D., F. G. Fernald and C. L. Frush. "Combined Use of Lidar and Numerical Diffusion Models to Estimate the Quantity and Dispersion of Volcanic Eruption Clouds in the Stratosphere: Vulcan Fuego, 1974, and Augustine, 1976," J. Geophys. Res., 82, (1977) 1783-1786.